SCIENTIFIC REPORTS

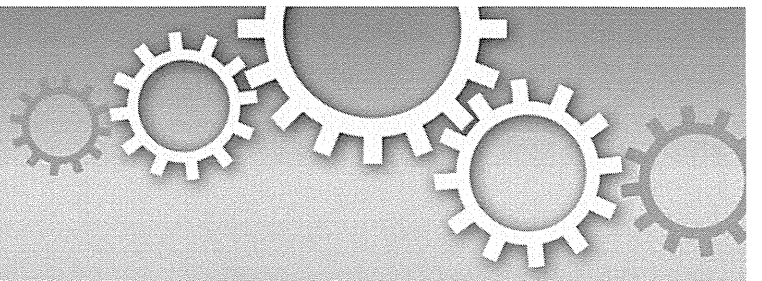

OPEN

SUBJECT AREAS:
BLOOD PROTEINS
DIAGNOSTIC MARKERS

Received
8 July 2014

Accepted
11 August 2014

Published
29 August 2014

Correspondence and requests for materials should be addressed to K.U. (k-ueda@ims.u-tokyo.ac.jp)

# Antibody-coupled monolithic silica microtips for highthroughput molecular profiling of circulating exosomes

Koji Ueda[1,2], Nobuhisa Ishikawa[3], Ayako Tatsuguchi[2], Naomi Saichi[1,2], Risa Fujii[1,2] & Hidewaki Nakagawa[2]

[1]Division of Biosciences, Functional Proteomics Center, Graduate School of Frontier Sciences, the University of Tokyo, Tokyo, Japan, [2]Laboratory for Genome Sequencing Analysis, Center for Integrated Medical Sciences, RIKEN, Tokyo, Japan, [3]Department of Molecular and Internal Medicine, Hiroshima University, Hiroshima, Japan.

Exosome-mediated signal transportation plays a variety of critical roles in cancer progression and metastasis. From the aspect of cancer diagnosis, circulating exosomes are ideal resources of biomarkers because molecular features of tumor cells are transcribed on them. However, isolating pure exosomes from body fluids is time-consuming and still major challenge to be addressed for comprehensive profiling of exosomal proteins and miRNAs. Here we constructed anti-CD9 antibody-coupled highly porous monolithic silica microtips which allowed automated rapid and reproducible exosome extraction from multiple clinical samples. We applied these tips to explore lung cancer biomarker proteins on exosomes by analyzing 46 serum samples. The mass spectrometric quantification of 1,369 exosomal proteins identified CD91 as a lung adenocarcinoma specific antigen on exosomes, which was further validated with CD9-CD91 exosome sandwich ELISA measuring 212 samples. Our simple device can promote not only biomarker discovery studies but also wide range of omics researches about exosomes.

Lung cancer is the leading cause of cancer-related mortality worldwide, accounting for 1,475,117 deaths in 2011 (Global Health Observatory Data Repository, World Health Organization). The high mortality is mainly attributable to a late-stage diagnosis and the lack of effective treatments. Indeed, by means of current cancer screening tests, only 30% of patients are diagnosed at an early disease stage and present surgically resectable tumors[1]. Therefore development of novel biomarkers and establishment of blood-based early detection system for lung cancer is crucial in order to improve clinical outcome and overall survival rate.

Recently biological significance and clinical utility of exosomes have been extensively discussed. Particularly contribution of tumor-derived exosomes to the formation of metastatic microenvironments is one of the most fundamental functions of them, which would provide a better understanding for cancer metastasis and even new therapeutic strategies to prevent metastasis[2–4]. Exosome-mediated delivery of therapeutic RNAs has been already in a pioneering stage for cancer treatment[5,6]. In the field of cancer diagnosis, exosomes are also fascinating targets for biomarker discovery due to their molecular characteristics[7–9]. In principle, a set of molecules expressed in original solid tumor cells would be detectable as exosomal components in blood circulation. Despite the theoretical feasibility of exosomal biomarkers, difficulties in exosome isolation from biological fluids have significantly hindered effective discovery of biomarker candidates. In fact, although ultracentrifugation-based methods are the most common strategies to isolate exosomes from serum samples[10], the reproducibility, processing time, and purity are not appropriate for biomarker screening studies dealing with a lot of clinical samples quantitatively[11].

In the present study, we established an antibody-assisted exosome purification tips by immobilizing anti-CD9 antibody to Mass Spectrometric Immunoassay (MSIA) monolith pipette tips. This multi-channeled platform effectively streamlined proteome-wide mass spectrometric profiling of serum exosomes and allowed accurate statistical identification of lung cancer-specific exosomal proteins. We further constructed exosome sandwich ELISA assays for large-scaled replication study to validate screening reliability for an identified exosome surface antigen CD91.

## Results

**Isolation of serum exosomes by anti-CD9-MSIA tips.** To perform reproducible and high-purity separation of exosomes from serum, we employed the antibody-immobilized low back pressure monolithic tips on automated

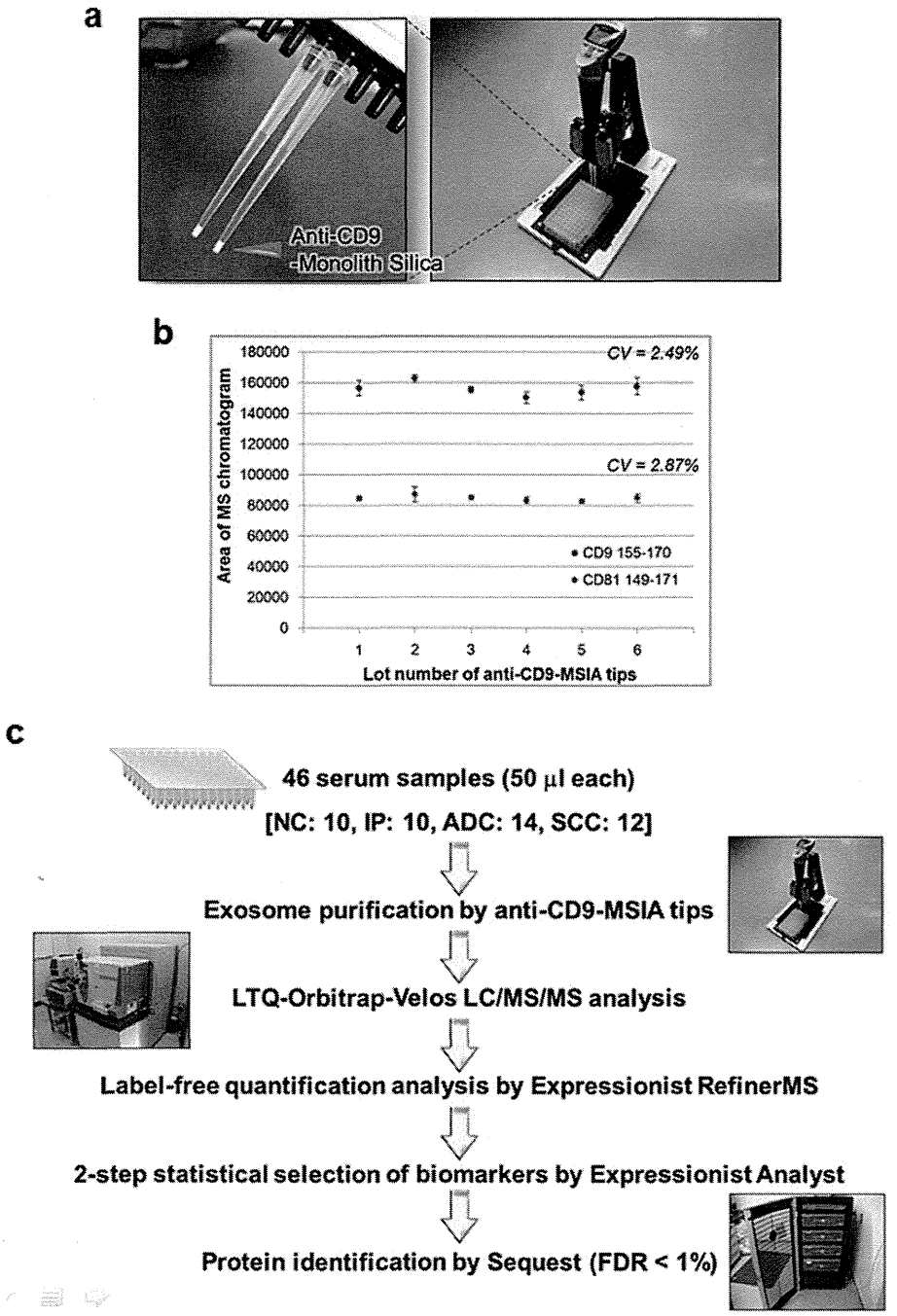


**Figure 1 | Schematic view of exosomal biomarker discovery workflow.** (a) Magnified picture of anti-CD9 MSIA tips (left) and a dedicated holding fixture (right). Pictures were taken by authors. (b) Exosome fractions were purified from a pooled serum sample using 6 independent anti-CD9-MSIA tips and analyzed by LC/MS/MS in triplicated measurements. The coefficient of variation (CV) of peak intensities corresponding to CD9 155-170 peptide (GLAGGVEQFISDICPK, m/z = 845.9266) or CD81 149-171 peptide (TFHETLDccGSSTLTALTTSVLK, m/z = 848.0733) was shown. (c) Exosomes were isolated from 46 serum samples by anti-CD9 antibody-coupled monolith tips (anti-CD9-MSIA tips) on 12-channel automatic pipetting platform. The enriched exosome fractions were analyzed by LC/MS/MS and subjected to label-free quantification analysis by RefinerMS software on the Expressionist proteome server system. The quantified peptides underwent 2-step statistical analysis, composed of ANOVA and feature elimination method, and finally extracted biomarker candidate peptides were identified with Sequest database search. The identification threshold was set at false discovery rate (FDR) < 1%.

12-channel pipette system (Figure 1a), which allowed 30 minutes isolation of exosomes from 12 serum samples simultaneously. Here we selected a tetraspanin molecule CD9 as a target of exosome-capturing antibody due to its strong expression on the surface of exosomes secreted from diverse cell types[12]. In order to evaluate the reproducibility of anti-CD9-MSIA tips, exosomes were purified from a pooled serum sample using 6 independent tips and analyzed by LC/MS/MS in triplicated measurements (Figure 1b). The coefficient of variation (CV) of peak area corresponding to CD9 155-170 peptide (GLAGGVEQFISDICPK, m/z = 845.9266) or CD81 149-171 peptide (TFHETLDCCGSSTLTALTTSVLK, m/z = 848.0733), which was also known as a typical exosome marker molecule, was 2.49% or 2.87%, respectively, indicating that the error level in relative quantification analysis was small enough for reliable biomarker

Table 1 | Clinical Information of serum samples

| | Screening set (n = 46) | | | | Validation set (n = 212) | | | |
|---|---|---|---|---|---|---|---|---|
| | NC | IP | ADC | SCC | NC | IP | ADC | SCC |
| No. of samples | 10 | 10 | 14 | 12 | 54 | 19 | 105 | 34 |
| Age (average) | 44.7 | 71.6 | 61.5 | 65.3 | 40.2 | 65.7 | 64.4 | 68.8 |
| Gender (female/male) | 4/6 | 3/7 | 6/8 | 2/10 | 29/25 | 5/14 | 35/70 | 7/27 |
| TNM stage | | | | | | | | |
| I | | | 0 | 0 | | | 12 | 5 |
| II | | | 0 | 0 | | | 10 | 0 |
| III | | | 4 | 5 | | | 27 | 18 |
| IV | | | 10 | 7 | | | 56 | 11 |

NOTE: NC, normal control; IP, interstitial pneumonia; ADC, adenocarcinoma; SCC, squamous cell carcinoma.

identification. Then we next isolated serum exosomes from 10 normal controls (NC), 10 interstitial pneumonia patients (IP), 14 lung adenocarcinoma patients (ADC), and 12 lung squamous cell carcinoma patients (SCC) using anti-CD9-MSIA tips. Purified exosomes were individually analyzed by LC/MS/MS system and subjected to statistical analysis as shown in Figure 1c.

**Proteome-wide overview of human serum exosomes.** The LC/MS/MS analysis of 46 serum samples (Table 1) and subsequent Sequest database search identified 1,369 non-redundant proteins (FDR < 1%, Supplementary Table 1). To assess the purity of anti-CD9-MSIA tip eluates, identified proteins were classified according to subcellular localizations (Figure 2a). The Cellular Component distribution by DAVID GO analysis illustrated highly-enriched 701 intracellular proteins (51.2%) and 290 plasma membrane proteins (21.2%), whereas only 135 extracellular (secreted) proteins (9.8%) were identified. These values clearly represented efficient enrichment of exosomes bearing original cell-derived cellular components. Importantly, most of serum abundant proteins such as albumin and IgG were effectively washed out during MSIA purification steps, which often hindered the sensitive detection of minor exosomal proteins. Moreover to elucidate physiological

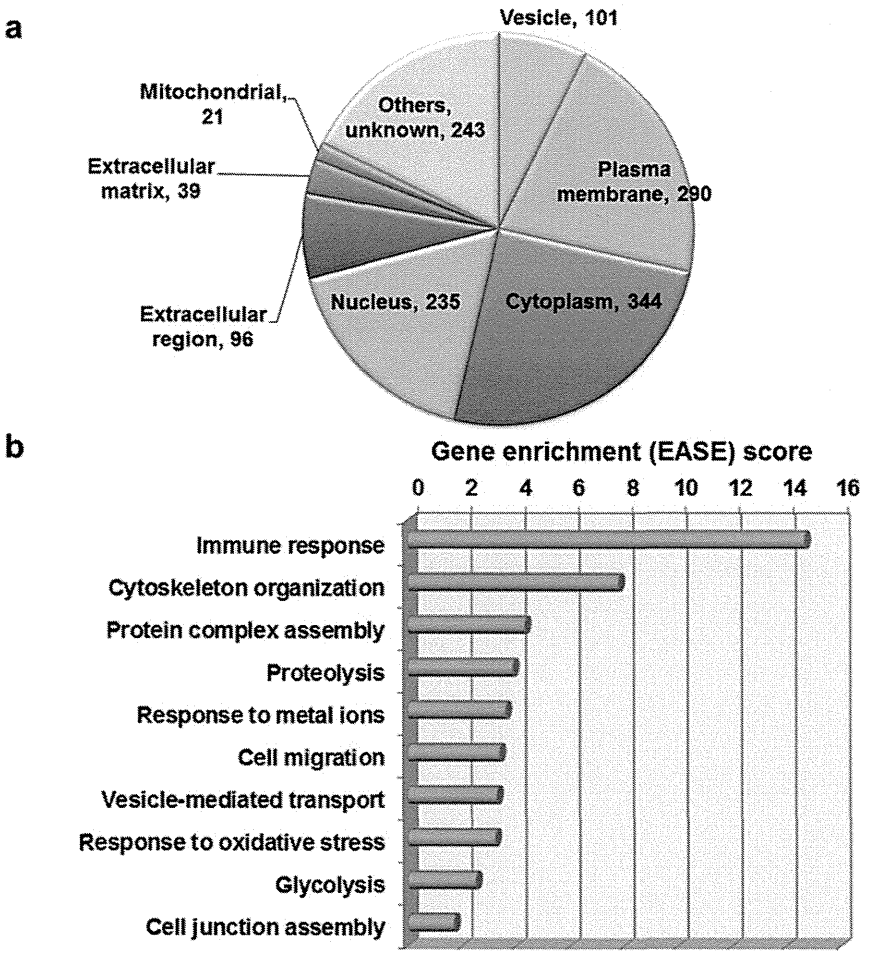


**Figure 2** | *Proteome-wide overview of 1,369 identified exosomal proteins.* (a) Distribution of protein subcellular localization was shown in a pie chart. (b) The Fisher Exact Statistics in DAVID system was used for functional annotation clustering analysis. The 10 enriched functions detected in 1,369 exosomal proteins were shown with Expression Analysis Systematic Explorer (EASE) scores.

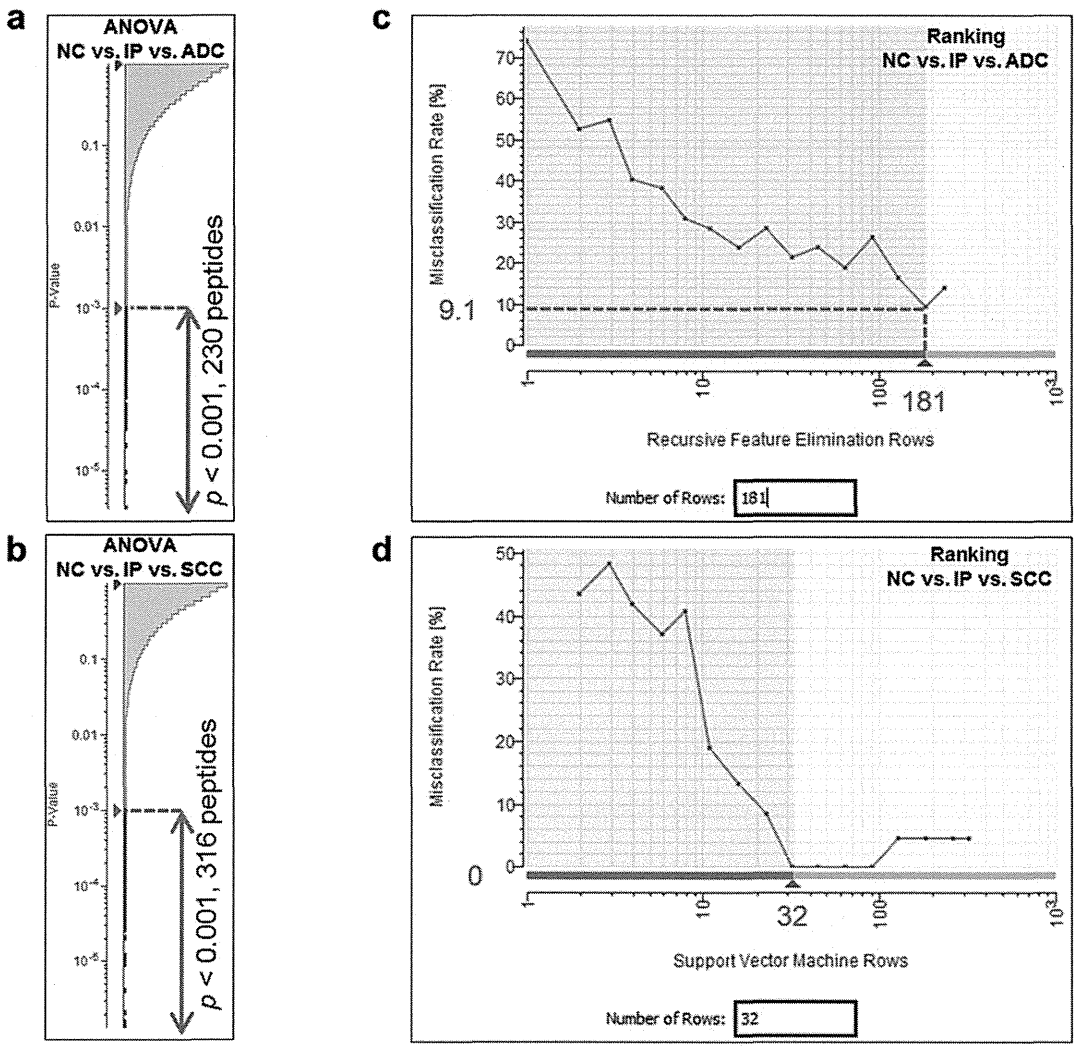


**Figure 3 | Two-step statistical selection of biomarker candidates.** For the first stage, 3-group ANOVA was performed to compare NC, IP, and ADC groups (a) or NC, IP, and SCC groups (b). Peptides satisfying the criterion $p < 0.001$ were used for the second Ranking selection. To calculate the minimum set of biomarkers which could provide the minimum misclassification rate, cross validation-based support vector machine-recursive feature elimination (SVM-RFE) method was used for comparison of NC, IP, and ADC groups (c). Similarly, SVM-SVM method was employed for comparison of NC, IP, and SCC groups (d). The number of selected biomarker candidates and the misclassification rate were shown. NC, normal control; IP, interstitial pneumonia; ADC, adenocarcinoma; SCC, squamous cell carcinoma.

functions of serum exosomes, Expression Analysis Systematic Explorer (EASE) scores were calculated[13,14] (Figure 2b). This functional estimation suggested the possible association of serum exosomes with immune regulations, cell-to-cell interactions, and stimulation responses, in addition to vesicle transport. These data would contribute to new revelations about the biological functions of not only tumor-derived exosomes but also normal exosomes.

Statistical identification of exosomal biomarkers for lung cancer. The label-free quantification analysis on the Expressionist Refiner MS module (Figure 1c and Supplementary Figure 1) quantified 113,582 non-redundant peptides from 46 serum samples. In the first statistical selection, 3-group ANOVA was used to roughly extract signature peptides specific to ADC patients (230 peptides, $p < 0.001$) or SCC patients (316 peptides, $p < 0.001$) as shown in Figure 3a or 3b, respectively. Here, to identify lung cancer specific exosomal biomarkers which don't react with inflammatory lung diseases such as interstitial pneumonia, IP patients were also considered as a non-cancer control group. For the second stage, cross validation-based feature elimination method was employed to compute the minimum biomarker sets which provided the least misclassification rates. Here support vector machine recursive feature elimination (SVM-RFE) method or SVM-SVM method defined 181 or 32 peptides as final candidate biomarker sets demonstrating 90.9% or 100% true prediction rate for ADC or SCC patients group (Figure 3c or 3d, respectively). By referring to protein identification data, 20 peptides derived from 18 proteins were identified (Figure 4 and Table 2). Among them, CD91, Integrin alpha-IIb, and CD317 were selected as favorable exosomal biomarker candidates because their expected localization was on the surface of exosomes and could be measured by exosome sandwich ELISA system (Figure 5a).

Validation experiment for CD91 by exosome sandwich ELISA. To assess the quantitative reproducibility of the label-free quantification results in our single-run screening analysis, as well as the clinical usefulness of a candidate biomarkers, we conducted further validation study by exosome sandwich ELISA using 212 independent serum samples (Table 1). Among three candidate biomarker proteins, we eventually succeeded to obtain good antibody and construct ELISA assay only for CD91. In this assay, we utilized anti-CD9 antibody as an exosome-capture antibody and

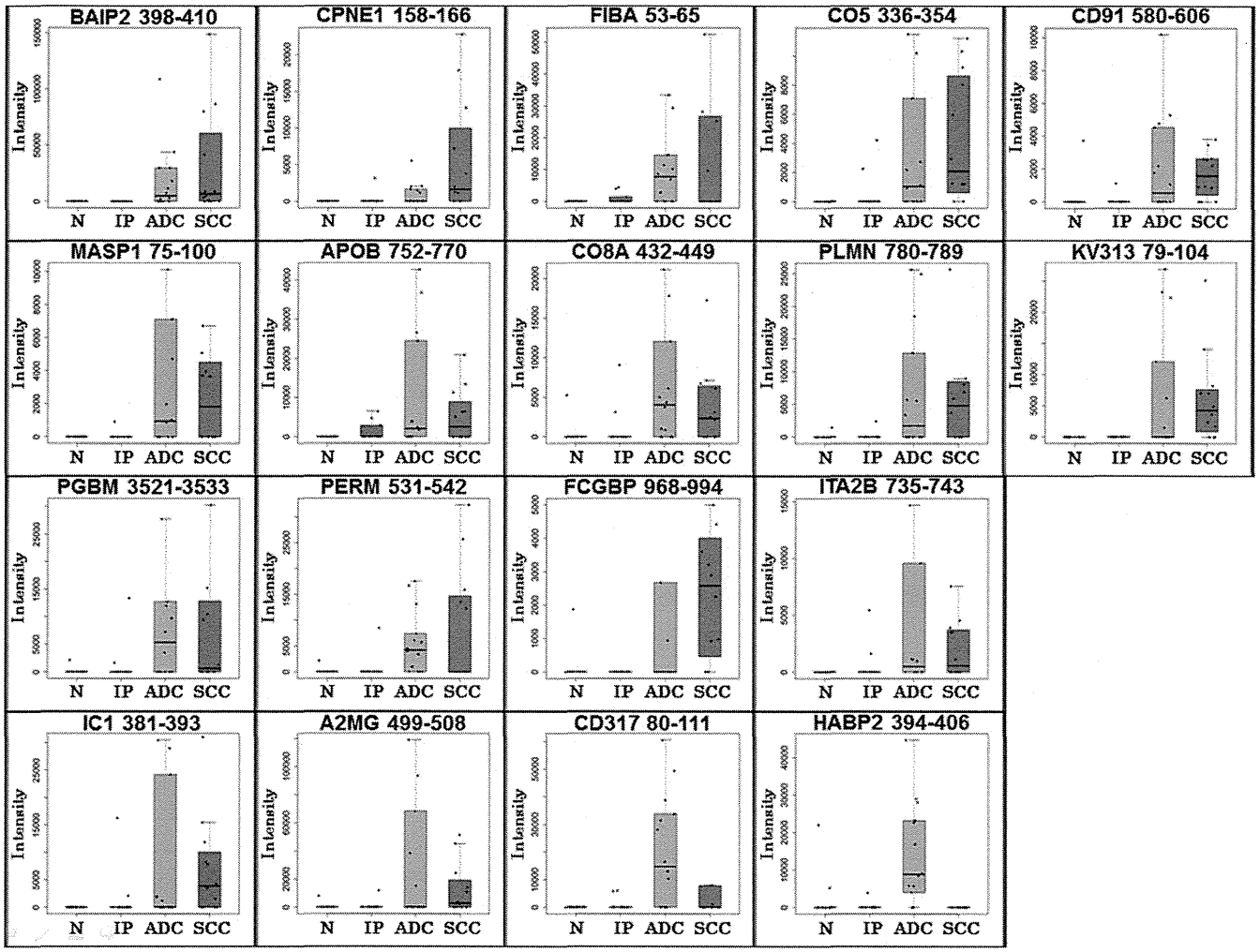


Figure 4 | Identified 18 exosomal biomarker candidates. The LC/MS/MS signal intensities for 18 biomarker candidates acquired from 46 cases were displayed in box plots. The UniProtKB entry protein names accompanied with amino acid numbers were shown over the box plots. N, normal control; IP, interstitial pneumonia; ADC, adenocarcinoma; SCC, squamous cell carcinoma.

biotinylated anti-CD9 or biotinylated anti-CD91 antibody as a detection antibody (Figure 5a). Since serum exosome concentrations, measured by CD9-CD9 sandwich ELISA, had drastic individual variability (Figure 5b), the measurements of CD9-CD91 sandwich ELISA were normalized by exosome concentrations (denoted by U/exosome in Figure 5c). We also tested a classical clinical biomarker CEA in the same sample set (Figure 5d) and compared the diagnostic efficacy to that of exosomal CD91. When we set the cut-off value at 2.04 U/exosome for exosomal CD91 and 5.0 ng/ml for CEA, exosomal CD91 showed significantly higher sensitivity for detecting stage-I, II ADC patients (54.5%) compared with CEA (22.7%), while the detection power of exosomal CD91 in stage-III, IV ADC patients (61.4%) was similar with that or CEA (66.3%). The false positive rate of exosomal CD91 in the control group (NC and IP, n = 73) were 11.0%, while that of CEA was 8.2%. These results indicated that exosomal CD91 possessed better potential for the early detection of lung ADC compared with CEA. On the other hand, exosomal CD91 might not be useful in the detection of SCC patients. In addition, we constructed a logistic regression model to evaluate the advantage of a combination of exosomal CD91 and CEA. The ROC curve analysis using control samples (NC and IP, n = 73) and all ADC samples (n = 105) in Figure 6a–c revealed that the combination biomarker effectively improved all of sensitivity (71.4%), specificity (91.8%), and area under the curve (0.882), compared with each single biomarker. Additionally, effects of age or gender on exosomal CD91 concentrations were assessed. The results indicated that exosomal CD91 was affected by neither age ($R^2$ = 0.0536, Supplementary Figure 2a) nor gender ($p$ = 0.299, Supplementary Figure 2b). These results suggested that exosomal CD91 was an independent predictor of lung ADC which could complement diagnostic power of CEA.

## Discussion

In recent years, physiological roles of secreted microvesicles, including exosomes, were actively studied mainly using cell culture supernatants (CCS). However studies on body fluid exosomes have been still at the stage of seeking appropriate technologies which allow high-purity isolation of exosomes. In fact, ultracentrifugal sedimentation methods, the most common techniques to purify exosomes[15], can not remove large size proteins (e.g. α2-macroglobulin, IgM, complement factors, and so on), aggregated proteins, circulating proteasome[16,17], and vault ribonucleoprotein particles[18] in serum because they have similar diameters (40 ~ 100 nm) and sedimentation coefficient to exosomes. Owing to these major contaminants, serum-derived proteins often occupy a great part of identified proteins by LC/MS/MS analysis of ultracentrifugal sedimentation samples (data not shown). In addition to the purity issue, throughput and reproducibility are also critical factors for the development of exosome isolation methods because biomarker screening studies or therapeutic target discovery studies usually deal with lots of clinical

Table 2 | 18 exosomal lung cancer biomarker candidates

| m/z | z | Protein Descriptions | UniProtKB entry | Protein Accessions | Sequence | XCorr |
|---|---|---|---|---|---|---|
| 713.401 | 2 | Brain-specific angiogenesis inhibitor 1-associated protein 2 | BAIP2 | Q9UQB8 | EGDLITLLVPEAR | 3.22 |
| 579.285 | 2 | Copine-1 | CPNE1 | Q99829 | SDPFLEFFR | 2.67 |
| 507.583 | 3 | Fibrinogen alpha chain | FIBA | P02671 | GLIDEVNQDFTNR | 4.54 |
| 1047.638 | 2 | Complement C5 | CO5 | P01031 | LNLVATPLFLKPGIPYPIK | 3.79 |
| 1011.136 | 3 | Prolow-density lipoprotein receptor-related protein 1 | CD91/LRP1 | Q07954 | DGIHNVEGVAVDWMGDNLYWTDDGPK | 4.57 |
| 953.123 | 3 | Mannan-binding lectin serine protease 1 | MASP1 | P48740 | ETTDTEQTPGQEVVLSPGSFMSITFR | 5.28 |
| 1027.069 | 2 | Apolipoprotein B-100 | APOB | P04114 | ILGEELGFASLHDLQLLGK | 5.58 |
| 1100.068 | 2 | Complement component C8 alpha chain | CO8A | P07357 | YNPVVIDFEMQPIHEVLR | 5.22 |
| 619.324 | 2 | Plasminogen | PLMN | P00747 | FVTWIEGVMR | 3.31 |
| 481.584 | 3 | Basement membrane-specific heparan sulfate proteoglycan core protein | PGBM | P98160 | IAHVELADAGQYR | 3.52 |
| 670.872 | 2 | Myeloperoxidase | PERM | P05164 | IGLDLPALNMQR | 3.30 |
| 1441.657 | 2 | IgGFc-binding protein | FCGBP | Q9Y6R7 | VPSSYAEALCGLCGNFNGDPADDLALR | 4.49 |
| 512.332 | 2 | Integrin alpha-IIb | ITA2B | P08514 | IVLLDVPVR | 3.21 |
| 1020.122 | 3 | Ig kappa chain V-III region HIC | KV313 | P18136 | LEPEDFAVYYCQQYGSSPWTFGQGTK | 4.62 |
| 742.352 | 2 | Plasma protease C1 inhibitor | IC1 | P05155 | VTTSQDMLSIMEK | 2.65 |
| 542.811 | 2 | Alpha-2-macroglobulin | A2MG | P01023 | GHFSISIPVK | 3.09 |
| 1141.520 | 3 | Bone marrow stromal antigen 2 | CD317/BST2 | Q10589 | GFQDVEAQAATCNHTVMALMASLDAEKAQGQK | 3.11 |
| 727.377 | 2 | Hyaluronan-binding protein 2 | HABP2 | Q14520 | LKPVDGHcALESK | 2.95 |

NOTE: m/z, mass/charge; z, charge; XCorr, cross-correlation score from Sequest database search.

specimens. To satisfy these technological requirements, we established a rapid, reproducible, and high-quality isolation device by integrating exosome capture antibody, low pressure monolith tips, and 12-well automatic pipet. Since the MSIA tips are also compatible with commercial 96-well automatic pipetting workstations, our method is applicable for larger (> 100 cases) sample set studies. In the present study, we used anti-CD9 antibody to capture exosomes in both MSIA tip devices and exosome sandwich ELISA system. Although CD9 is one of the most well-known exosome markers, the expression level of CD9 might vary by tissues[19] or disease state[20,21]. These facts indicate that a single use of anti-CD9 antibody could provide proteome profiles for only a limited proportion of serum exosomes. Therefore effective combination of antibodies specific to various exosome markers (e.g. CD63 or CD81) would improve the comprehensiveness of exosome profiling studies.

From the proteome-wide biomarker screening of 46 serum samples, we eventually identified 18 biomarker candidate proteins in Figure 4 and Table 2. Concerning subcellular localizations of them, 6 proteins express in intracellular regions (BAIP2 in peripheral membrane area; copine-1 on vesicle membrane; myeloperoxidase in lysosome; CD91, integrin alpha-IIb, and CD317 on plasma membrane), however, other 13 proteins were known as major serum proteins. Although the number of identified extracellular proteins was small as shown in Figure 2a, the purification efficiency of anti-CD9-MSIA tip was still considered incomplete. In order for further improvement of this device, we're now optimizing the coating agents for monolith polymer in the tips to minimize non-specific binding of serum proteins. Because the amount of exosome-derived proteins is indeed ultratrace level compared to serum major proteins, the improvement of exosome purification efficiency could significantly increase the chances of detecting minor exosomal antigens associated with cancer development or progression. More effective and inexpensive exosome isolation method could also promote development of mass spectrometric multiplexed biomarker diagnosis measuring two or more exosomal biomarkers simultaneously by MRM/SRM assay.

In this report, we showed that CD91 expression was significantly elevated on exosomes in especially lung ADC patients' sera. The detection power for limited number of early stage patients (n = 22) was also higher than existing biomarker CEA (Figure 5c and 5d), but so far we can conclude that the exosomal CD91 assay could detect at least a large cancer burden. For functional consideration of CD91, this molecule is a type-1 transmembrane receptor which mediates ligand endocytosis in clathrin-coated pits and cargo trafficking to lysosomes[22,23]. Another fundamental role of CD91 is reported as a signaling receptor regulating cytokine secretion, phagocytosis and migration of cells in the immune system[24,25]. Notably, with regard to cancer, no or very low expression of CD91 in lung cancer cells was observed in tissues from ADC patients with poor clinical outcome, while strong staining patterns of CD91 were observed in stromal cells surrounding cancer cells from 94/111 ADC patients[26]. Combined with our results, high level of serum CD91-expressing exosomes would be originally secreted from stromal cells surrounding lung cancer cells. Since construction of tumor microenvironments is one of the most well-established functions of exosomes[3], inhibiting production or function of CD91-positive exosomes might lead to suppression of lung cancer progression. Therefore inhibitors of CD91, which interfere ligand binding, such as the receptor-associated protein (RAP), suramin, α2-macroglobulin, and lactoferrin[27] would be useful for investigating the association of exosomal CD91 and lung cancer. In contrast to CD91, another candidate of exosomal biomarker CD317 was already confirmed as a potential therapeutic target for lung cancer[28]. Due to its nature of lung cancer specific expression, chimeric or humanized antibody drugs were developed and tested in clinical trials[29]. This evidence indicated that the lung ADC cells directly release high level of CD317-positive exosomes in blood circulation.

Thus in addition to identification of biomarker candidates, our anti-CD9 MSIA tips can provide diverse novel knowledge about human exosomes. More comprehensive information will be also obtained by replacing the epitope of immobilized antibody with other exosomal surface antigens such as CD63, CD81, tetraspanin-9, or tetraspanin-14.

## Methods

Serum samples. Serum samples from lung cancer patients (n = 165), interstitial pneumonia patients (n = 29), and normal controls (n = 64) were collected in Hiroshima University Hospital within the same period. All samples were collected

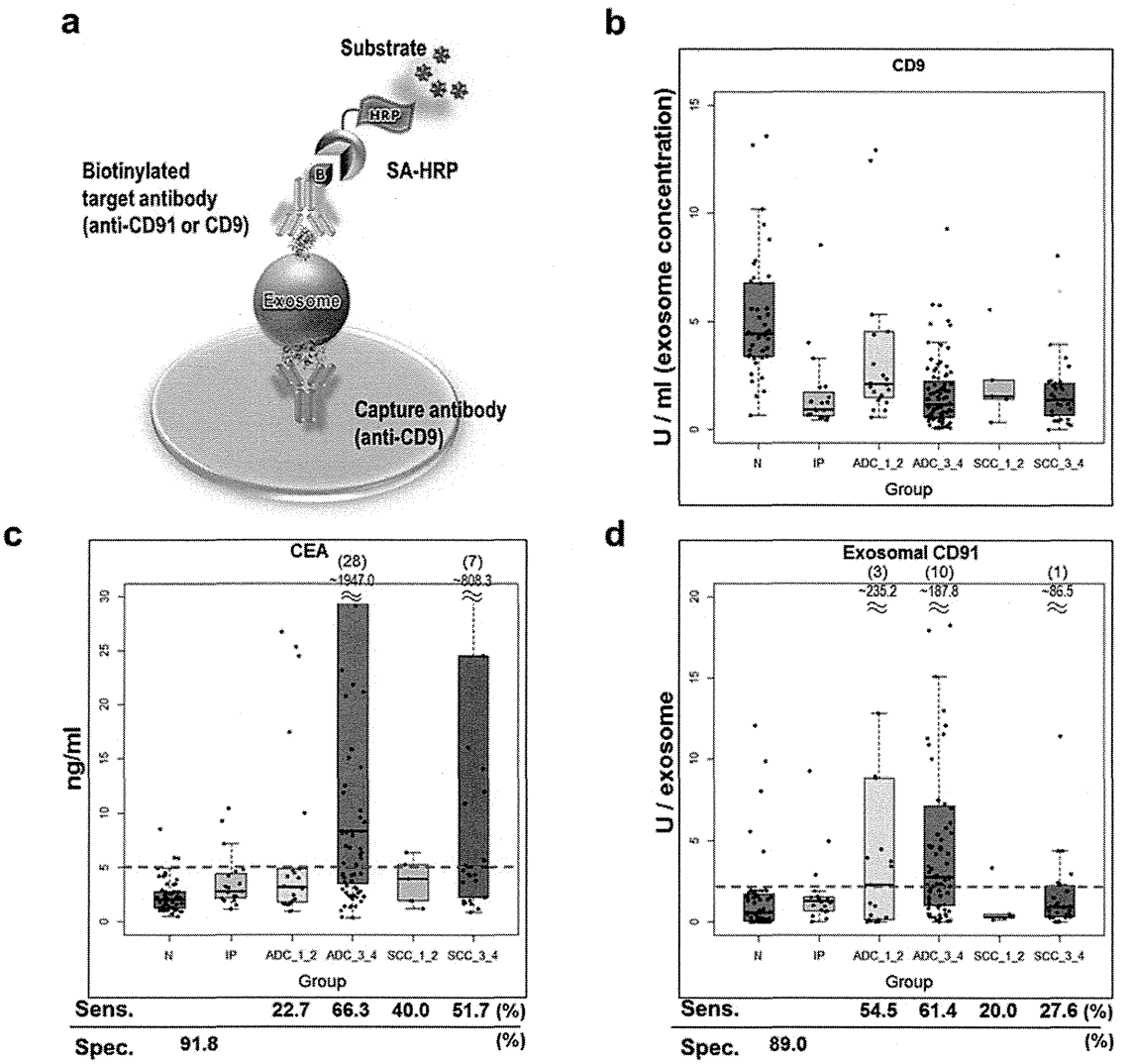


Figure 5 | Exosome sandwich ELISA-based validation experiment for CD91. (a) Principle of exosome sandwich ELISA. SA-HRP, streptavidin-horseradish peroxidase. Using 212 independent serum samples, exosomal CD91 and CEA concentrations were measured. (b) Serum exosome concentrations were determined by CD9-CD9 sandwich ELISA. (c) CEA concentrations were measured by commercial ELISA kits. (d) Exosomal CD91 concentrations were determined by CD9-CD91 sandwich ELISA. The values were normalized with exosome concentrations calculated in (b). Red lines indicate the cut-off values for CEA at 5.0 ng/ml (c) or exosomal CD91 at 2.04 U/exosome (d). The sensitivity (Sens.) for each lung cancer sub-group and specificity (Spec.) were shown below the box plots. N, normal control; IP, interstitial pneumonia; ADC_1_2, stage-I, II adenocarcinoma; ADC_3_4, stage-III, IV adenocarcinoma; SCC_1_2, stage-I, II squamous cell carcinoma; SCC_3_4, stage-III, IV squamous cell carcinoma.

from untreated patients at the initial visit to hospital. The nonanticoagulated blood samples were collected and allowed to clot at room temperature for 1–2 hours. Sera were then separated by centrifugation at 1500 rpm for 15 min and stored frozen at −80°C. Written informed consents were obtained from all participants. This study was approved by The Ethical Committee of RIKEN (Approval code: Yokohama H20-12) and The Ethical Committee of Hiroshima University Hospital. All experiments were performed in accordance with relevant guidelines and regulations.

Exosome purification by anti-CD9 MSIA tips. All procedures were performed on Novus-i 12-channel electronic pipettes and adjustable pipette stand (Thermo Fisher Scientific, Waltham, Massachusetts, USA). The MSIA D.A.R.T.'s, Protein G tips (Thermo Fisher Scientific) were equilibrated with 300 μl PBS × 10 cycles prior to 25 μl × 100 cycles of immobilization of 1 μg anti-CD9 antibody (provided by Shionogi & Co., Ltd., Osaka, Japan) in 50 μl PBS. After crosslinking with 0.25 mM BS3 (Thermo Fisher Scientific) in PBS (100 μl × 100 cycles), reaction was quenched with 50 mM ethanolamine-HCl (pH 8.0) (100 μl × 100 cycles). Following 300 μl × 10 cycles of equilibration in PBS, the anti-CD9-MSIA tips were incubated with 350 μl of seven-fold diluted serum samples by 300 μl × 100 cycles pipetting. Tips were washed three times by 300 μl × 25 cycles pipetting in PBS. Finally captured exosomes were eluted by 20 μl × 100 cycles pipetting in 30 μl of [8M Urea, 50 mM ammonium bicarbonate] solution.

After reduction with 5 mM TCEP at 37°C for 30 minutes and alkylation with 25 mM iodoacetamide at room temperature for 45 minutes, samples were diluted 7 times with 50 mM ammonium bicarbonate. Proteins were digested by Immobilized Trypsin beads (Thermo Fisher Scientific) in a 96-well filter plate with continuous shaking at 37°C for 6 hours. Tryptic digests were desalted by Oasis HLB 96-well μElution Plate (Waters Corporation, Milford, Massachusetts, USA) and subjected to LC/MS/MS analysis.

LC/MS/MS analysis. The dried peptide samples were resuspended in 2% acetonitrile with 0.1% trifluoroacetic acid and analyzed by LTQ-Orbitrap-Velos mass spectrometer (Thermo Fisher Scientific) combined with UltiMate 3000 RSLC nano-flow HPLC system (DIONEX Corporation, Sunnyvale, California, USA). Samples were separated on 75 μm × 150 mm $C_{18}$ tip-column (Nikkyo Technos, Tokyo, Japan) using solvent A [0.1% formic acid] and solvent B [0.1% formic acid in acetonitrile] with multistep linear gradient of solvent B 6.4 to 30% for 95 minutes and 30 to 95% for 10 minutes at a flow rate 250 nl/min. The eluted peptides were ionized with the spray voltage 2000 V and MS data was acquired in a data-dependent fragmentation method in which the survey scan was acquired between m/z 400 to 1600 at the resolution 60,000 with automatic gain control (AGC) target value of 1.0 × 106 ion counts. The top-20 intense precursor ions in each survey scan were subjected to low resolution MS/MS acquisitions using normal CID scan mode with AGC target value of 5,000 ion counts in the linear ion trap.

The protein identification analysis was performed by SEQUEST database search on Proteome Discoverer 1.3 software (Thermo Fischer Scientific). The MS/MS spectra were searched against human protein database SwissProt 2013_03 (20,255 sequences)

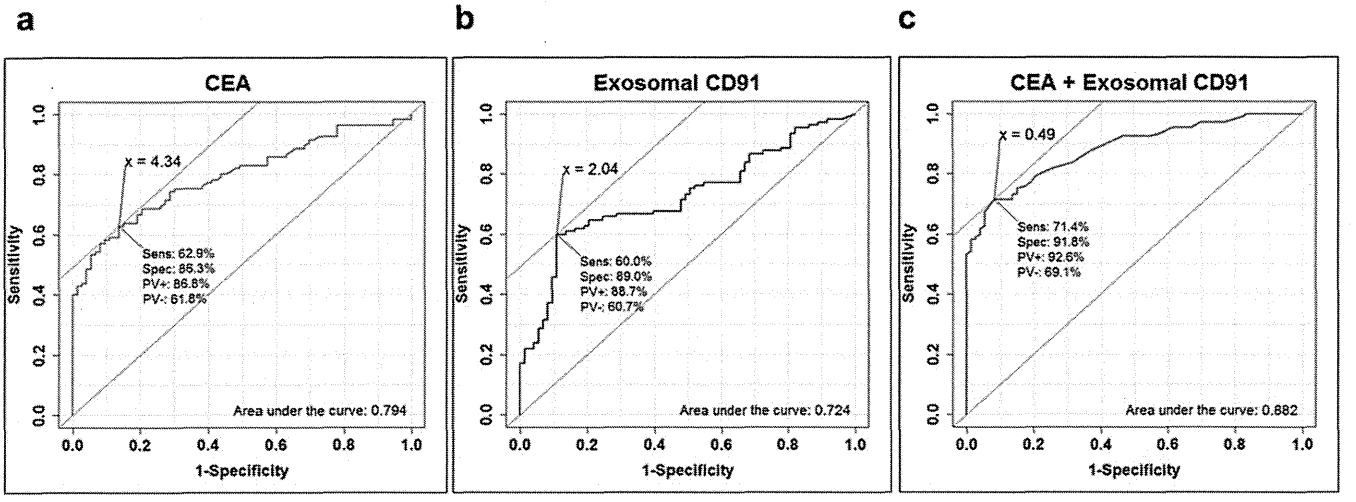


Figure 6 | ROC curve analysis for exosomal CD91 and CEA. ROC curves for CEA (a), exosomal CD91 (b), and logistic regression-based combination marker CEA + exosomal CD91 (c) were depicted by R. The diagnostic efficiencies between NC + IP (n = 73) and lung ADC patients (n = 105) were evaluated. The cut-off value was set at the point whose distance from the (sensitivity, specificity) = (1, 1) reached the minimum. The sensitivity (Sens), specificity (Spec), positive predictive value (PV+), negative predictive value (PV-), and area under the curve (AUC) were shown on each graph.

using search parameters as follows: Enzyme Name = Semitrypsin, Precursor Mass Tolerance = 10 ppm, Fragment Mass Tolerance = 0.8 Da, Dynamic Modification = Oxidation (Met), and Static Modification = Carbamidomethyl (Cys). False discovery rate of 0.01 and Peptide Rank of 1 were set for peptide identification filters. The gene ontology analysis was performed on EASE (Expression Analysis Systematic Explorer, version 2.0) (http://www.geneontology.org/) to compute the overrepresented functional categories in "Cellular Component," and "Molecular Function".

Label-free quantification analysis on Expressionist server. The LC/MS/MS data set was loaded to Expressionist RefinerMS module (Genedata AG, Basel, Switzerland) for data processing and label-free quantification analysis. The whole workflow of RefinerMS software was shown in Supplementary Figure S1. The Spectrum Grid was set at every 10 data points on 2D MS chromatogram planes (x = m/z and y = RT). The Structure Removal was sequentially performed with RT = 2 scans and m/z = 6 points in the first and second Chemical Noise Subtraction, respectively, followed by the third Subtraction using RT Window = 500 scans and Quantile = 90%. After forth Subtraction with RT = 2 scans, signals with intensity < 2,000 were clipped off by Intensity Thresholding. Finally further Structure Removals with RT = 2 scans and m/z = 5 points were run as the fifth and sixth Chemical Noise Subtractions, respectively.

Then Chromatogram Grid was set at every 10 scans on noise-subtracted data, followed by Chromatogram RT Alignment using parameters: m/z Window = 11 points, RT Window = 11 scans, Gap Penalty = 1, RT Search Interval = 2 minutes, and Alignment Scheme = pairwise alignment based tree. Next, the Summed Peak Detection Activity detected the peaks on a temporarily-averaged chromatogram with parameters as follows: Summation Window = 20 scans, Overlap = 10, Minimum Peak Size = 6 scans, Maximum Merge Distance = 1 data points, Gap/Peak Ratio = 5, Method = curvature-based peak detection, Peak Refinement Threshold = 5, and Consistency Filter Threshold = 1. Finally Summed Isotope Clustering Activity grouped isotopic peaks derived from single molecule into an isotope cluster. Here parameters were used as follows: Minimum Charge = 1, Maximum Charge = 6, Maximum Missing Peaks = 0, First Allowed Gap Position = 10, Ionization = protonation, RT Tolerance = 0.1 minute, m/z Tolerance = 0.01 Da, and Minimum Cluster Size Ratio = 0.5.

Statistical analysis on Expressionist Analyst. Two-step statistical selection was employed for the effective identification of biomarker set. In the first stage, 3-group ANOVA was performed to roughly extract the candidates showing significantly distinct expression level among three clinical groups ($p < 0.001$). Next the minimum combination of biomarkers which provided the best classification rate was estimated by the Support Vector Machine-Recursive Feature Elimination (SVM-RFE) Ranking method in the Expressionist Analyst module (Genedata AG). SVM-RFE is an iterative algorithm that works backward from an initial set of statistical features. As a classifier, SVM was used for inferring decision rules. RFE was used as a ranking method which iteratively dropped the 10% peptides with the lowest weights in each step. Finally a Line Plot visualizer was returned displaying the average misclassification rate. Each classifier was represented by a line and the optimal classifier and biomarker peptide set size for the chosen ranking method could be read off.

Exosome sandwich ELISA assay. The 250 ng/well of anti-CD9 antibody was immobilized to Nunc MaxiSorp flat-bottom 96 well plate (Thermo Fischer Scientific). The blocking solution (150 μl/well of 5% BSA in PBS) was then added and incubated on the plate shaker at ambient temperature for 60 minutes. After 3 times wash with PBS, [5 μl serum + 95 μl PBS] or [30 μl serum + 70 μl PBS] was loaded to the upper 48 wells or the lower 48 wells, respectively. Following 5 hours incubation, plates were washed three times by PBS. The 100 μl/well of biotinylated anti-CD9 antibody (125 ng/ml) or biotinylated anti-CD91 antibody (500 ng/ml, Abcam, Cambridge, UK) in 1% BSA was loaded to the upper 48 wells or the lower 48 wells, respectively. After 60 minutes incubation, plates were washed three times with PBS and then covered with 100 μl/well of 1×HRP-Streptavidin (Abcam) in 1% BSA solution. After 30 minutes incubation, plates were washed three times with PBS and covered with 100 μl/well of TMB Ready Solution (Thermo Fischer Scientific). The reaction was stopped after 10 minutes incubation using 100 μl/well of 2N HCl. The OD at 450 nm was immediately measured. The concentration data from CD9-CD9 and CD9-CD91 ELISA assays were normalized with gradient curves (5, 10, 15, 20, and 25 μl) obtained from a common pleural effusion sample. Finally CD91 concentrations were normalized with exosome concentration calculated with CD9-CD9 ELISA above.

Box plot analysis and ROC curve analysis. The intensities of mass spectrum peaks corresponding to candidate biomarker peptides were displayed by box plot using R algorithm. For each study the box represents the middle half of the distribution of the data points stretching from the 25th percentile to the 75th percentile. The line across the box represents the median. The lengths of the lines above and below the box are defined by the maximum and minimum data point values, respectively, that lie within 1.5 times the spread of the box. ROC curves were also depicted by R. The cut-off value was set at the point whose distance from the (sensitivity, specificity) = (1, 1) reached the minimum. The sensitivity (Sens), specificity (Spec), positive predictive value (PV+), negative predictive value (PV-), and are under the curve (AUC) were shown on each graph.


1. Lehtio, J. & De Petris, L. Lung cancer proteomics, clinical and technological considerations. *J Proteomics* 73, 1851–1863 (2010).
2. Luga, V. *et al.* Exosomes mediate stromal mobilization of autocrine Wnt-PCP signaling in breast cancer cell migration. *Cell* 151, 1542–1556 (2012).
3. Peinado, H. *et al.* Melanoma exosomes educate bone marrow progenitor cells toward a pro-metastatic phenotype through MET. *Nature medicine* 18, 883–891 (2012).
4. Kosaka, N. *et al.* Neutral sphingomyelinase 2 (nSMase2)-dependent exosomal transfer of angiogenic microRNAs regulate cancer cell metastasis. *J Biol Chem* 288, 10849–10859 (2013).
5. Grapp, M. *et al.* Choroid plexus transcytosis and exosome shuttling deliver folate into brain parenchyma. *Nature communications* 4, 2123 (2013).
6. El-Andaloussi, S. *et al.* Exosome-mediated delivery of siRNA in vitro and in vivo. *Nat Protoc* 7, 2112–2126 (2012).
7. Sandoval, M. *et al.* The glycolytic enzyme aldolase C is up-regulated in rat forebrain microsomes and in the cerebrospinal fluid after repetitive fluoxetine treatment. *Brain research* 1520, 1–14 (2013).
8. Tanaka, Y. *et al.* Clinical impact of serum exosomal microRNA-21 as a clinical biomarker in human esophageal squamous cell carcinoma. *Cancer* 119, 1159–1167 (2013).
9. Khan, S. *et al.* Plasma-derived exosomal survivin, a plausible biomarker for early detection of prostate cancer. *PLoS One* 7, e46737 (2012).
10. Lasser, C. Identification and analysis of circulating exosomal microRNA in human body fluids. *Methods in molecular biology* 1024, 109–128 (2013).

11. Witwer, K. W. *et al.* Standardization of sample collection, isolation and analysis methods in extracellular vesicle research. *Journal of extracellular vesicles* 2, 20360 (2013).
12. Keller, S., Sanderson, M. P., Stoeck, A. & Altevogt, P. Exosomes: from biogenesis and secretion to biological function. *Immunology letters* 107, 102–108 (2006).
13. Ford, G., Xu, Z., Gates, A., Jiang, J. & Ford, B. D. Expression Analysis Systematic Explorer (EASE) analysis reveals differential gene expression in permanent and transient focal stroke rat models. *Brain research* 1071, 226–236 (2006).
14. Tan, P. K. *et al.* Evaluation of gene expression measurements from commercial microarray platforms. *Nucleic acids research* 31, 5676–5684 (2003).
15. Taylor, D. D., Zacharias, W. & Gercel-Taylor, C. Exosome isolation for proteomic analyses and RNA profiling. *Methods in molecular biology* 728, 235–246 (2011).
16. Sixt, S. U. & Dahlmann, B. Extracellular, circulating proteasomes and ubiquitin - incidence and relevance. *Biochimica et biophysica acta* 1782, 817–823 (2008).
17. Egerer, K. *et al.* Circulating proteasomes are markers of cell damage and immunologic activity in autoimmune diseases. *The Journal of rheumatology* 29, 2045–2052 (2002).
18. Kedersha, N. L., Heuser, J. E., Chugani, D. C. & Rome, L. H. Vaults. III. Vault ribonucleoprotein particles open into flower-like structures with octagonal symmetry. *The Journal of cell biology* 112, 225–235 (1991).
19. Huang, C. *et al.* MRP-1/CD9 and KAI1/CD82 expression in normal and various cancer tissues. *Int J Oncol* 11, 1045–1051 (1997).
20. Miyake, M. *et al.* Motility related protein 1 (MRP-1/CD9) expression: inverse correlation with metastases in breast cancer. *Cancer Res* 55, 4127–4131 (1995).
21. Sauer, G. *et al.* Progression of cervical carcinomas is associated with down-regulation of CD9 but strong local re-expression at sites of transendothelial invasion. *Clin Cancer Res* 9, 6426–6431 (2003).
22. Strickland, D. K., Gonias, S. L. & Argraves, W. S. Diverse roles for the LDL receptor family. *Trends in endocrinology and metabolism: TEM* 13, 66–74 (2002).
23. Weaver, A. M., McCabe, M., Kim, I., Allietta, M. M. & Gonias, S. L. Epidermal growth factor and platelet-derived growth factor-BB induce a stable increase in the activity of low density lipoprotein receptor-related protein in vascular smooth muscle cells by altering receptor distribution and recycling. *J Biol Chem* 271, 24894–24900 (1996).
24. Yoon, C. *et al.* Low-density Lipoprotein Receptor-related Protein 1 (LRP1)-dependent Cell Signaling Promotes Axonal Regeneration. *J Biol Chem* 288, 26557–26568 (2013).
25. Stiles, T. L. *et al.* LDL receptor-related protein-1 is a sialic-acid-independent receptor for myelin-associated glycoprotein that functions in neurite outgrowth inhibition by MAG and CNS myelin. *Journal of cell science* 126, 209–220 (2013).
26. Meng, H. *et al.* Stromal LRP1 in lung adenocarcinoma predicts clinical outcome. *Clin Cancer Res* 17, 2426–2433 (2011).
27. Vassiliou, G., Benoist, F., Lau, P., Kavaslar, G. N. & McPherson, R. The low density lipoprotein receptor-related protein contributes to selective uptake of high density lipoprotein cholesteryl esters by SW872 liposarcoma cells and primary human adipocytes. *J Biol Chem* 276, 48823–48830 (2001).
28. Wang, W. *et al.* HM1.24 (CD317) is a novel target against lung cancer for immunotherapy using anti-HM1.24 antibody. *Cancer immunology, immunotherapy : CII* 58, 967–976 (2009).
29. Wang, W. *et al.* Chimeric and humanized anti-HM1.24 antibodies mediate antibody-dependent cellular cytotoxicity against lung cancer cells. *Lung cancer* 63, 23–31 (2009).


## Acknowledgments

This study was performed as a research program of the Project for Development of Innovative Research on Cancer Therapeutics (P-Direct), Ministry of Education, Culture, Sports, Science and Technology of Japan. We thank Dr. Hiroyuki Okamoto and Dr. Hikaru Sonoda from Shionogi & Co., Ltd. for kindly providing anti-CD9 antibody.

## Author contributions

K.U. designed the study and developed the method. K.U., N.I., A.T., N.S. and R.F. performed experiments and analyzed data. K.U. and H.N. interpreted the results and wrote the manuscript.

## Additional information

Supplementary information accompanies this paper at http://www.nature.com/scientificreports

Competing financial interests: The authors declare no competing financial interests.

How to cite this article: Ueda, K. *et al.* Antibody-coupled monolithic silica microtips for high throughput molecular profiling of circulating exosomes. *Sci. Rep.* 4, 6232; DOI:10.1038/srep06232 (2014).

Cancer Letters 351 (2014) 126–133

Contents lists available at ScienceDirect

Cancer Letters

journal homepage: www.elsevier.com/locate/canlet

# SMYD2-dependent HSP90 methylation promotes cancer cell proliferation by regulating the chaperone complex formation

Ryuji Hamamoto [a,b,*], Gouji Toyokawa [b], Makoto Nakakido [a], Koji Ueda [c], Yusuke Nakamura [a]

[a] Section of Hematology/Oncology, Department of Medicine, The University of Chicago, 5841 S. Maryland Ave., MC2115 Chicago, IL 60637, United States
[b] Laboratory of Molecular Medicine, Human Genome Center, Institute of Medical Science, The University of Tokyo, 4-6-1 Shirokanedai, Minato-ku, Tokyo 108-8639, Japan
[c] Laboratory for Biomarker Development, Center for Genomic Medicine, RIKEN, 4-6-1 Shirokanedai, Minato-ku, Tokyo 108-8639, Japan

ARTICLE INFO

*Article history:*
Received 13 January 2014
Received in revised form 30 April 2014
Accepted 11 May 2014

*Keywords:*
SMYD2
Human carcinogenesis
HSP90
Non-histone protein methylation

ABSTRACT

Heat shock protein 90 (HSP90) is a highly conserved molecular chaperone that facilitates the maturation of a wide range of proteins, and it has been recognized as a crucial facilitator of oncogene addiction and cancer cell survival. Although HSP90 function is regulated by a variety of post-translational modifications, the physiological significance of methylation has not fully been elucidated. Here we demonstrate that HSP90AB1 is methylated by the histone methyltransferase SMYD2 and that it plays a critical role in human carcinogenesis. HSP90AB1 and SMYD2 can interact through the C-terminal region of HSP90AB1 and the SET domain of SMYD2. Both *in vitro* and *in vivo* methyltransferase assays revealed that SMYD2 could methylate HSP90AB1 and mass spectrometry analysis indicated lysines 531 and 574 of HSP90AB1 to be methylated. These methylation sites were shown to be important for the dimerization and chaperone complex formation of HSP90AB1. Furthermore, methylated HSP90AB1 accelerated the proliferation of cancer cells. Our study reveals a novel mechanism for human carcinogenesis via methylation of HSP90AB1 by SMYD2, and additional functional studies may assist in developing novel strategies for cancer therapy.



## Introduction

HSP90 is an evolutionarily conserved molecular chaperone that is known to participate in stabilizing and activating more than 200 proteins, referred to as HSP90 "clients", many of which are essential for constitutive cell signaling and adaptive responses to various stresses [1,2]. To accomplish this task, HSP90 and proteins called co-chaperones form the dynamic complex known as the HSP90 chaperone machine [3]. Cancer cells use the HSP90 chaperone machinery to protect an array of mutated and overexpressed oncoproteins from misfolding and degradation. Therefore, HSP90 is recognized as a crucial facilitator of oncogene addiction and cancer survival [4]. HSP90 function is regulated by various post-translational modifications such as acetylation, phosphorylation and nitrosylation. Phosphorylation of HSP90AB1's charged linker regulates the interaction with the client aryl hydrocarbon receptor (AHR). Substitution of Ser 225 and Ser 254, which are located in a central domain and phosphorylation targets, to Ala increases HSP90 binding affinity to AHR, suggesting that phosphorylation negatively regulates complex formation [5]. In addition, HSP90 phosphorylation facilitates client maturation. SRC-dependent phosphorylation of Tyr 300 in HSP90AB1 increases the association of the chaperone with the client endothelial nitric oxide synthase (eNOS) on activation of vascular endothelial growth signaling [6]. Moreover, acetylation of Lys 294 in a middle domain by an unknown acetylase inhibits the co-chaperone binding and maturation of client proteins [7,8]; histone deacetylase 6 deacetylates this residue *in vivo* [9]. Furthermore, nitrosylation of Cys 597 in the HSP90AB1 CTD is known to inhibit eNOS activation *in vivo* [10,11], and *in vitro* S-nitrosylation inhibits HSP90 ATPase activity and shifts the conformational equilibrium of the chaperone cycle. Other post-translational modifications have been reported for HSP90, but physiological significance of methylation still remains unclear.

SMYD2 was first identified as one of the SMYD family members, containing the SET domain and the MYND domain [12]. SMYD2 was reported to methylate histone H3K36 and H3K4, and functions as a transcriptional regulator in cooperation with the Sin3A and HDAC1 histone deacetylase complex [12,13]. We recently demonstrated that SMYD2 was overexpressed in various types of cancer and played a crucial role in the cell cycle regulation of cancer cells through methylation of the tumor suppressor RB1 [14]. Besides

* Corresponding author at: Section of Hematology/Oncology, Department of Medicine, The University of Chicago, 5841 S. Maryland Ave., MC2115 Chicago, IL 60637, United States. Tel.: +1 773 702 0933.
*E-mail address:* rhamamoto@medicine.bsd.uchicago.edu (R. Hamamoto).

http://dx.doi.org/10.1016/j.canlet.2014.05.014
0304-3835/

histone and RB1 proteins, SMYD2 also methylates the tumor suppressor p53 and represses its tumor suppression function [15]. Additionally, Komatsu et al. reported elevated expression of SMYD2 in esophageal squamous cell carcinoma, and that SMYD2 positivity was independently associated with a worse outcome of patients in the multivariate analysis [16]. These results indicate that deregulation of SMYD2 may be one of the critical factors in human carcinogenesis.

In this study, we show that SMYD2 methylates HSP90AB1 and regulates the dimerization and chaperone complex formation. Our findings demonstrate a novel post-translational modification of HSP90, which may play a critical role in human carcinogenesis.

## Materials and methods

### *Cell culture*

SW780, RT4, HeLa and 293T cells were from American Type Culture Collection (ATCC) in 2001 and 2003, and tested and authenticated by DNA profiling (Supplementary Table 1). All cell lines were grown in monolayers in appropriate media: Dulbecco's Modified Eagle's Medium (D-MEM) for 293T cells; Eagle's minimal essential medium (E-MEM) for HeLa cells; Leibovitz's L-15 for SW780 cells; McCoy's 5A medium for RT4 cells supplemented with 10% fetal bovine serum and 1% antibiotic/antimycotic solution (Sigma–Aldrich, St. Louis, MO, USA). All cells were maintained at 37 °C in humid air with 5% $CO_2$ condition (293T, HeLa and RT4) or without $CO_2$ (SW780). Cells were transfected with FuGENE6™ (Roche Applied Science, Penzberg, Germany) according to manufacturer's protocols.

### *Immunoprecipitation*

293T cells were seeded at a density of $5 \times 10^5$ cells on a 100-mm dish. The next day, the cells were transfected with expression vector constructs using FuGENE6, and after 48 h, transfected 293T cells were washed with PBS and lysed in CelLytic™ M Cell Lysis Reagent (Sigma–Aldrich, St Louis, MO) containing complete protease inhibitor cocktail (Roche Applied Science). 500 μg of whole-cell extract were incubated with anti-FLAG M2 agarose (Sigma–Aldrich) for 1 h at 4 °C. After the beads were washed 3 times with 1 ml of TBS buffer (pH 7.6), the FLAG-tagged proteins bound to the beads were eluted by boiling in Lane Marker Sample Buffer (Thermo Fisher Scientific, Waltham, MA). Samples were then subjected to SDS–PAGE, and detected by silver staining or western blot.

### *Mass spectrometry*

HSP90AB1 samples reacted with SMYD2 were separated on SDS–PAGE and stained with CBB. The excised HSP90AB1 bands were reduced in 10 mM tris (2-carboxyethyl)phosphine (Sigma–Aldrich) with 50 mM ammonium bicarbonate (Sigma–Aldrich) for 30 min at 37 °C and alkylated in 50 mM iodoacetamide (Sigma–Aldrich) with 50 mM ammonium bicarbonate for 45 min in the dark at 25 °C. Trypsin GOLD (Promega) solution was added with the enzyme to protein ratio at 1/50 (w/w) and incubated at 37 °C for 16 h. The resulting peptides were extracted from gel fragments and separated on a 0.1 × 200 mm homemade $C_{18}$ column using 45 min linear gradient from 2% to 35% acetonitrile in 0.1% formic acid with flow rate at 200 nl/min. The eluting peptides were analyzed with HCTultra ETD II mass spectrometer (Bruker Daltonics, Bremen, Germany). The acquired MS and CID MS/MS spectra were processed with Compass DataAnalysis 4.0 (Bruker Daltonics) and BioTools 3.1 software (Bruker Daltonics), followed by the database search on in-house Mascot server ver. 2.3.01 (Matrix Science). We accepted the peptide identifications satisfying the Expectation value less than 0.05 in Mascot Database search.

### *Western blot*

Whole cell lysates were prepared from the cells with RIPA-like buffer or CelLytic™ M Cell Lysis Reagent (Sigma–Aldrich) containing complete protease inhibitor cocktail (Roche Applied Science) and total protein or immunoprecipitated samples were transferred to nitrocellulose membrane. The membrane was probed with anti-SMYD2 (sc-79084; Santa Cruz Biotechnology, Santa Cruz, CA), anti-HSP90 (sc-13119; Santa Cruz Biotechnology), anti-HSP90AB1 (ab53497, Abcam), anti-α-Tubulin (CP-06, Millipore), anti-ACTB (I-19, Santa Cruz Biotechnology), anti-FLAG (F7425; Sigma–Aldrich), anti-HA (Y-11; Santa Cruz Biotechnology), anti-HOP (SRA-1500; Stressgen Bioreagents), anti-Cdc37 (sc-5617; Santa Cruz Biotechnology), anti-p23 (ab2814; Abcam), anti-SMYD2 (#9734, Cell Signaling Technology, Danvers, MA), anti-ERBB2 (#2248, Cell Signaling Technology), anti-CDK4 (#12790, Cell Signaling Technology) and anti-HSP90AB1 (#5087, Cell Signaling Technology) antibodies. An anti-mono-methylated HSP90AB1K574 antibody was made by Cell Engineering Corporation. Protein bands were detected by incubating with horseradish peroxidase-conjugated antibodies (GE Healthcare, Little Chalfont, UK) and visualizing with Enhanced Chemiluminescence (GE Healthcare).

### *Immunocytochemistry*

Cells were fixed with PBS (−) containing 4% paraformaldehyde for 20 min, and rendered permeable with PBS (−) containing 0.1% Triton X-100 at room temperature for 2 min. Subsequently, the cells were covered with PBS (−) containing 3% bovine serum albumin for 1 h at room temperature to block non-specific hybridization, and then were incubated with mouse anti-HSP90 antibody (sc-13119, Santa Cruz Biotechnology) at a 1:1000 dilution ratio and goat anti-SMYD2 (sc-79084) at a 1:500 dilution ratio. After washing with PBS (−), cells were stained by an Alexa Fluor® 488-conjugated anti-goat secondary antibody (Life Technologies, Carlsbad, CA) or an Alexa Fluor® 594-conjugated anti-mouse secondary antibody (Life Technologies) at a 1:1000 dilution ratio. Nuclei were counter-stained with 4′,6′-diamidine-2′-phenylindole dihydrochloride (DAPI). Fluorescent images were obtained under a TCS SP2 AOBS microscope (Leica Mycrosystems, Wetzlar, Germany).

### *In vitro methyltransferase assay*

*In vitro* methyltransferase assays were described previously [17,18]. Briefly, recombinant HSP90AB1 protein was incubated with recombinant SMYD2 enzyme using 1 μCi S-adenosyl-L-[methyl-$^3$H]-methionine (SAM; PerkinElmer) as the methyl donor in a mixture of 10 μl of methylase activity buffer (50 mM Tris–HCl at pH8.8, 10 mM DTT and 10 mM $MgCl_2$), for 2 h at 30 °C. After boiling in sample buffer, the samples were subjected to SDS–PAGE, and visualized by fluorography and Ponceau S.

### *In vivo labeling*

*In vivo* labeling was performed as described previously [19]. Cells were starved for 1 h in methionine-free medium, including cycloheximide (100 μg/ml) and chloramphenicol (40 μg/ml). They were then labeled with L-[methyl-$^3$H] methionine (10 μCi/ml, Perkin Elmer) for 5 h. FLAG-Mock, SMYD2 (WT) or SMYD2 (ΔNHSC/GEEV) was immunoprecipitated with an anti-HSP90 antibody (Santa Cruz Biotechnology) and methylated HSP90 was visualized by fluorography.

### *siRNA transfection*

siRNA oligonucleotide duplexes were purchased from Sigma–Aldrich for targeting the human *SMYD2* transcripts. siEGFP control, which targets enhanced green fluorescent protein (GFP), was used as control siRNAs. The siRNA sequences are described in Supplementary Table 2. siRNA duplexes (100 nM final concentration) were transfected into bladder and lung cancer cell lines with Lipofectamine 2000 (Life Technologies) [20,21].

### *Quantitative real-time PCR (qRT-PCR)*

For quantitative RT-PCR reactions, specific primers for all human *GAPDH* (housekeeping gene), *ERBB2* and *CDK4* were designed. PCR reactions were performed using the LightCycler® 480 System (Roche Applied Science) following the manufacture's protocol.

### *In vitro cross-linking assay*

*In vitro* cross-linking was performed as described previously [22]. After *in vitro* methyltransferase assay in the presence or absence of SMYD2, HSP90AB1 was incubated with 94.7 mM PBS (pH 7.4) and 10 mM $BS^3$ (Thermo Scientific) for 30 min at room temperature. The cross-linking reaction was quenched by adding 1 M Tris–HCl. After boiling in sample buffer, each reaction mixture was subjected to SDS–PAGE, followed by western blot analysis using an anti-HSP90 antibody (Santa Cruz Biotechnology). After the western blot, the membrane was stained by Ponceau S.

### *In vivo cross-linking assay*

HeLa cells were seeded at a density of $5 \times 10^5$ cells on a 100-mm dish. The next day, the cells were treated with siSMYD2. 24 h after siRNA treatment, the cells were transfected with pCAGGS-n3FC-HSP90AB1 (WT) or pCAGGS-n3FC-HSP90AB1 (K531A/K574A). 24 h after transfection, EMEM was replaced by Dulbecco's Modified Eagle's Limiting Medium (DMEM-LM) (Thermo Fisher Scientific) containing L-Photo-Leucine and L-Photo-Methionine (Thermo Fisher Scientific), subjected to UV irradiation (Stratalinker® UV Crosslinker, American Laboratory Trading, 10800 J). Then, the cells were harvested and total protein (5 μg) was transferred to nitrocellulose membrane, followed by SDS–PAGE and western blot analysis using

anti-FLAG (Sigma–Aldrich), anti-SMYD2 (Santa Cruz Biotechnology) and anti-ACTB (Santa Cruz Biotechnology) antibodies. Protein bands were detected as described above.

*Primer sequences*

Oligonucleotides to construct mammalian expression vectors and expression vectors for recombinant proteins in *Escherichia coli* are described in Supplementary Tables 3 and 4, respectively.

## Results

*SMYD2 forms a complex with HSP90AB1*

In order to clarify a novel substrate of SMYD2-dependent methylation, we attempted to screen an interacting partner(s) of SMYD2. We used 293T cells that were transfected with a FLAG-Mock or a FLAG-SMYD2 vector. Immunoprecipitation (IP) and subsequent mass spectrometry (MS) analysis indicated HSP90AB1 to be a candidate of a SMYD2-interacting partner (Fig. 1A). Since the HSP90 protein has been considered to play critical roles in human cancer by chaperoning many oncoproteins and facilitating their function [1], we examined the functional relationship between SMYD2 and HSP90AB1. The interaction between SMYD2 and HSP90AB1 was confirmed by co-immunoprecipitation (Fig. 1B and C). We then attempted to determine the region of SMYD2 that binds to HSP90AB1 and constructed plasmid clones designed to express different portions of SMYD2. Co-immunoprecipitation analysis (Fig. 1D) indicated that SMYD2 bound to HSP90AB1 through a central region including a part of the SET domain (Fig. 1E). With regard to the binding of HSP90AB1 to SMYD2, we found the C-terminal region to be important for interaction with SMYD2 (Fig. 2A and B). In addition, immunocytochemical analysis revealed their co-localization of these two proteins in the cytoplasm (Fig. 2C). These results imply that SMYD2 forms a complex with HSP90AB1.

*SMYD2 methylates HSP90AB1*

HSP90 protein is known to have multiple post-translational modifications (PTMs) [7,11,23,24], but the biological significance of methylation still remains unclear. Therefore, we examined whether SMYD2 could methylate HSP90AB1 and affect its functions. First, we performed an *in vitro* methyltransferase assay and found that HSP90AB1 is methylated by SMYD2 in a dose-dependent manner (Fig. 3A). We further validated the methylation of HSP90AB1 by SMYD2 in 293T cells that were transfected with a FLAG-Mock vector, a FLAG-SMYD2 (WT) vector or a FLAG-SMYD2 (ΔNHSC/GEEV) vector, which was designed to express enzyme-dead SMYD2 [14]. *In vivo* labeling experiments revealed a strong signal corresponding to methylated HSP90 in SMYD2-transfected cells, but a very weak signal in mock- or enzyme-dead SMYD2-transfected cells (Fig. 3B, Supplementary Fig. 1). We then tried to determine which portion of HSP90AB1 is methylated by SMYD2 and prepared several deletion mutants of recombinant HSP90AB1 protein. *In vitro* methyltransferase assays using these constructs (Fig. 3C and D) revealed that the C-terminal portion of GST-HSP90AB1 (500–724 aa) contained a methylated residue(s) by SMYD2. Subsequent LC-MS/MS analysis identified lysines 531 and 574 to be candidate methylation targets by SMYD2 (Fig. 4A and B). Substitution of K574 to alanine decreased the signal of SMYD2-dependent HSP90AB1 methylation, and the methylation signal was further reduced when using both K531 and K574 substituted HSP90AB1 (Fig. 4C). This result was confirmed using a partial HSP90AB1 (500–724 aa) (Supplementary Fig. 2). Since these methylation sites are highly conserved from *Danio rerio* to *Homo sapiens*,

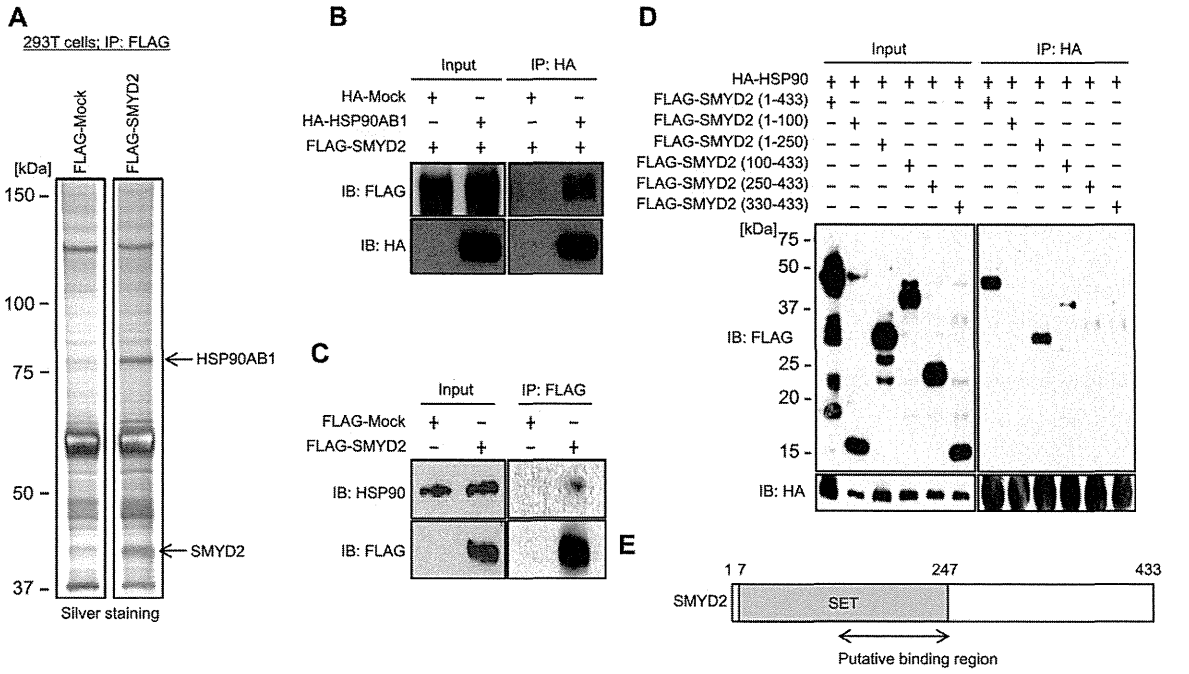


**Fig. 1.** SMYD2 forms a complex with HSP90AB1. (A) Silver staining of immunoprecipitates from FLAG-Mock or FLAG-SMYD2 expressing cells. 293T cells were transfected with FLAG-Mock or FLAG-SMYD2 and immunoprecipitated using an anti-FLAG M2 agarose. Immunoprecipitates were subject to SDS-PAGE and silver staining, followed by mass spectrometry. (B) 293T cells were co-transfected with HA-HSP90AB1 or HA-Mock and FLAG-SMYD2 expression vectors, and HA-immunoprecipitates were immunoblotted with anti-FLAG and anti-HA antibodies. (C) Interaction of FLAG-SMYD2 with endogenous HSP90 was confirmed by Western blot of FLAG-immunoprecipitates using anti-HSP90 and anti-FLAG antibodies. (D) The region including the SET domain of SMYD2 is required for interaction with HSP90AB1. 293T cells were co-transfected with an HA-HSP90AB1 expression vector and six different lengths of FLAG-SMYD2 expression vectors ([1–433], [1–100], [1–250], [100–433], [250–433] and [330–433]). Immunoprecipitation was performed using anti-HA agarose beads, and samples were immunoblotted with anti-FLAG and anti-HA antibodies. (E) Schematic representation of a binding region of SMYD2 to HSP90AB1.

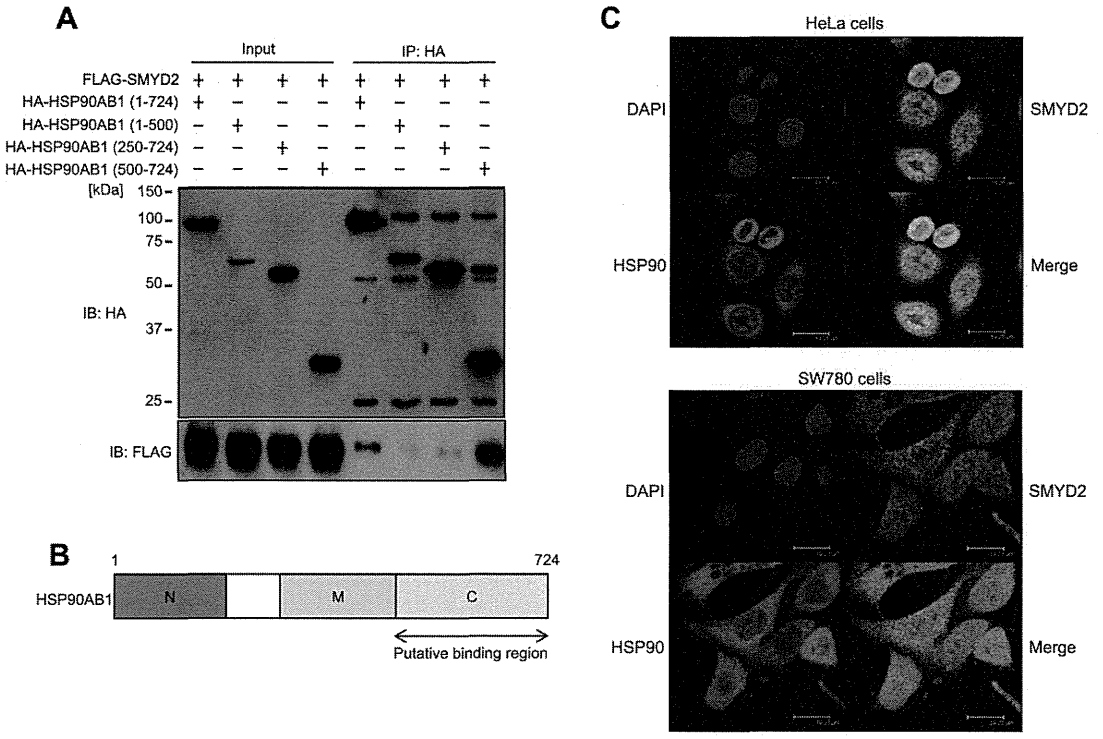


**Fig. 2.** SMYD2 binds to C-terminal region of HSP90AB1. (A) The C-terminal region of HSP90AB1 is required for binding to SMYD2. 293T cells were co-transfected with a FLAG-SMYD2 expression vector and four different lengths of HA-HSP90AB1 vectors ([1–724], [1–500], [250–724] and [500–724]). HA-immunoprecipitates were immunoblotted with anti-FLAG and anti-HA antibodies. (B) Schematic representation of a binding region of HSP90AB1 to SMYD2. (C) Co-localization of SMYD2 and HSP90AB1 in HeLa cells and SW780 cells. HeLa cells and SW780 cells were stained with anti-SMYD2 (Alexa Fluor® 488 [green]) and anti-HSP90 (Alexa Fluor® 594 [red]) antibodies, and DAPI (blue).

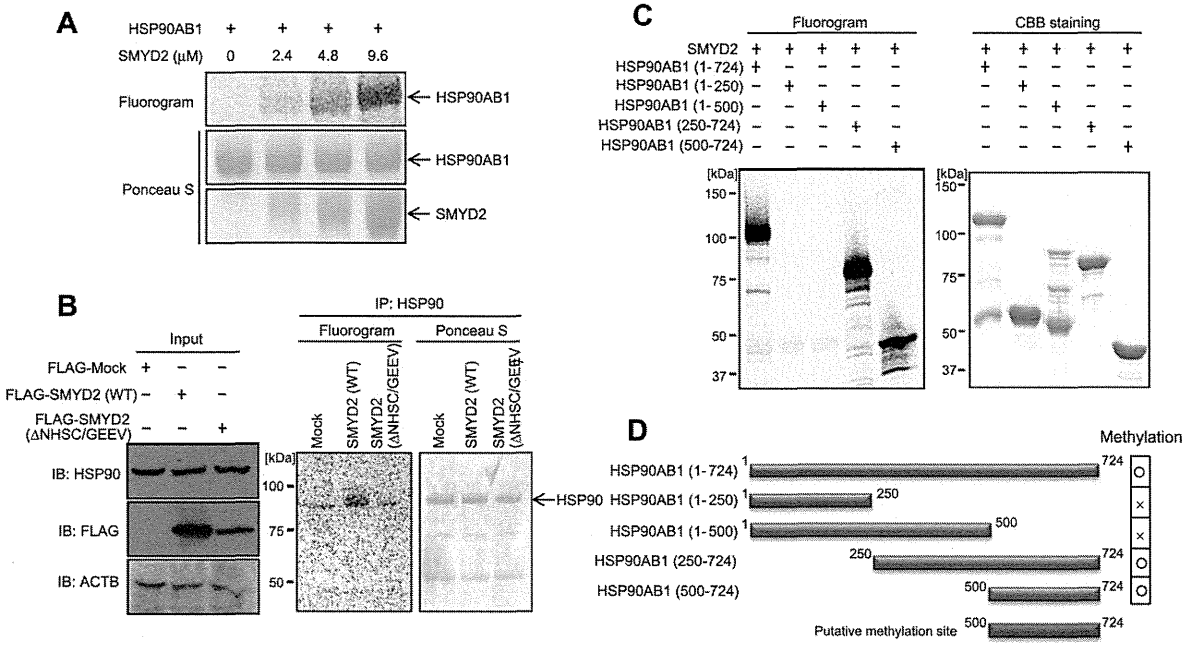


**Fig. 3.** SMYD2 methylates C-terminal region of HSP90AB1. (A) HSP90AB1 was methylated by SMYD2 in a dose-dependent manner. *In vitro* methyltransferase reaction was performed using purified His-HSP90AB1 and His-SMYD2 recombinant proteins, and methylated HSP90AB1 was visualized with fluorography. Amounts of loading protein were confirmed by staining the membrane with Ponceau S. (B) Methylation of HSP90 in human cells was confirmed by *in vivo* labeling experiment. 293T cells were transfected with FLAG-Mock, FLAG-SMYD2 (WT) or FLAG-SMYD2 (ΔNHSC/GEEV) expression vectors and treated with methionine-free medium, including cycloheximide and chloramphenicol. They were then labeled with L-[methyl-$^3$H] methionine for 5 h. Cell lysates were immunoprecipitated with an anti-HSP90 antibody, and methylated HSP90 was visualized by fluorography. The membrane was stained with Ponceau S and whole cell lysates were immunoblotted with anti-HSP90, anti-FLAG and anti-ACTB (an internal control) antibodies. (C) C-terminal region of HSP90AB1 (500–724) was methylated by SMYD2. *In vitro* methyltransferase assay was performed using five different lengths of GST-HSP90AB1 and His-SMYD2. Methylation activity was visualized by fluorography and CBB staining was conducted to confirm amounts of proteins. (D) Schematic representation of HSP90AB1 methylated by SMYD2. 500–724 part of HSP90AB1 (red) is a putative methylated region by SMYD2.

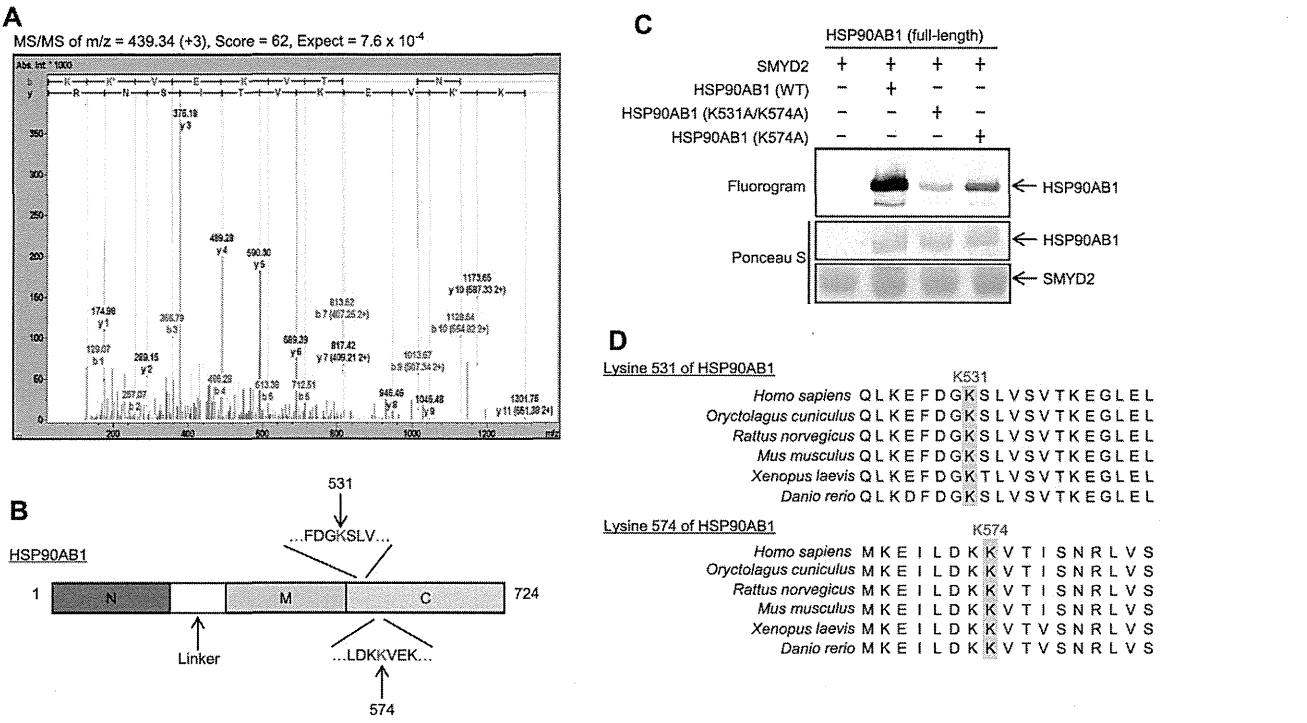


**Fig. 4.** Lys 531 and Lys 574 of HSP90AB1 were methylated by SMYD2. (A) The MS/MS spectrum corresponding to the mono-methylated HSP90AB1 573–583 peptide. The b- and y-type product ions are marked in the spectrum. The 14 Da increase of the Lys 574 residue was observed, demonstrating the mono-methylated Lys 574. Score and Expect show Mascot Ion Score and Expectation value in Mascot Database search results, respectively. (B) Schematic representation of methylation sites of HSP90AB1. (C) His-SMYD2 and full-length His-HSP90AB1 (WT, K531A/K574A and K574A) were reacted in the presence of S-adenosyl-L-[methyl-$^3$H] methionine, and the mixture was subjected to SDS–PAGE and visualized by fluorogram. The membrane was stained with Ponceau S. (D) Amino acid sequence of HSP90AB1. Lysines 531 and 574 are conserved across various species, including human (*Homo sapiens*), rabbit (*Oryctolagus cuniculus*), rat (*Rattus norvegicus*), mouse (*Mus musculus*), xenopus (*Xenopus laevis*) and zebrafish (*Danio rerio*).

it is very likely that methylation of these sites is critical for the regulation of HSP90AB1 functions (Fig. 4D).

### *SMYD2-dependent methylation alters the chaperone complex formation of HSP90AB1*

To analyze the effects of SMYD2-dependent methylation on the biological function of HSP90AB1, we performed a dimerization assay using bis[sulfosuccinimidyl] suberate ($BS^3$), a crosslinking reagent, by SDS–PAGE and western blot analysis. This experiment revealed the significant increase of the amount HSP90AB1 dimer when it was methylated, indicating that methylation of HSP90AB1 by SMYD2 enhanced dimerization of HSP90AB1 (Supplementary Fig. 3). We also validated the occurrence of methylation-dependent dimerization by SMYD2 in cultured cells. After siSMYD2 treatment that reduced the effects of endogenous SMYD2, we co-transfected a FLAG-HSP90AB1 (WT) vector and either a HA-Mock vector or a HA-SMYD2 vector into 293T cells. 48 h after transfection, we performed an *in vivo* cross-linking assay and found that the level of cross-linked HSP90AB1 was higher in the cells overexpressing SMYD2 than those transfected with mock (Supplementary Fig. 4). When we used the substituted HSP90AB1 (K531A/K574A), the amount of the dimerized HSP90AB1 was significantly diminished (Fig. 5A), further supporting the importance of methylation of lysines 531 and 574 in dimerization of HSP90AB1.

HSP90 exerts its chaperone functions together with co-chaperones [25,26]. Some PTMs are reported to alter the affinity of HSP90 to its co-chaperones [7,23,27]. Therefore, we investigated whether HSP90AB1 methylation affects the binding of HSP90AB1 to co-chaperones. A FLAG-HSP90AB1 (WT) vector or a FLAG-HSP90AB1 (K531A/K574A) vector was transfected into 293T cells, followed by immunoprecipitation and western blot analysis. We found that K531A/K574A substitution of HSP90AB1 reduced its interaction with HOP or Cdc37 (Fig. 5B). We also monitored methylation status of HSP90AB1 using a specific antibody recognizing mono-methylated HSP90AB1K574 (Fig. 5B and Supplementary Fig. 5). Taken together, SMYD2-dependent HSP90AB1 methylation appears to regulate the polymerization of HSP90AB1 and its chaperone complex formation.

### *Methylation of HSP90AB1 by SMYD2 promotes cancer cell growth*

It is known that HSP90 plays a crucial role in maintaining oncogenic protein homeostasis as a chaperone protein. To examine the effect of SMYD2-dependent methylation on the stability of client proteins, we conducted protein stability assays after knockdown of SMYD2. Western blot analysis was performed to monitor the stability of ERBB2 and CDK4, which are well-known HSP90 client oncoproteins. 48 h after treatment with siSMYD2, protein levels of both ERBB2 and CDK4 were significantly decreased in RT4 and SW780 cancer cells (Fig. 6A). Since mRNA expressions of both *ERBB2* and *CDK4* were unchanged, the decrease of ERBB2 and CDK4 protein levels was likely to be caused by degradation of these proteins (Fig. 6B), implying the significance of HSP90AB1 methylation by SMYD2 in the maintenance of these two proteins. Finally, to elucidate the significance of methylated HSP90AB1 in tumor growth, we generated stable transfectants of HeLa cells overexpressing FLAG-HSP90AB1 (WT) and FLAG-HSP90AB1 (K531A/K574A) because the dominant-negative experiment system of HSP90AB1 has already been established [28,29]. After confirming the stable expression of wild-type and substituted HSP90 proteins (Fig. 6C), we performed a growth assay using the stable cell lines. As a result, we found a growth promoting effect by wild-type HSP90AB1, not by substituted HSP90AB1, and we confirmed the result using two sets of independent cell lines (Fig. 6D, Supplementary Fig. 6). Taken together, these data suggest that SMYD2-dependent methylation appears to

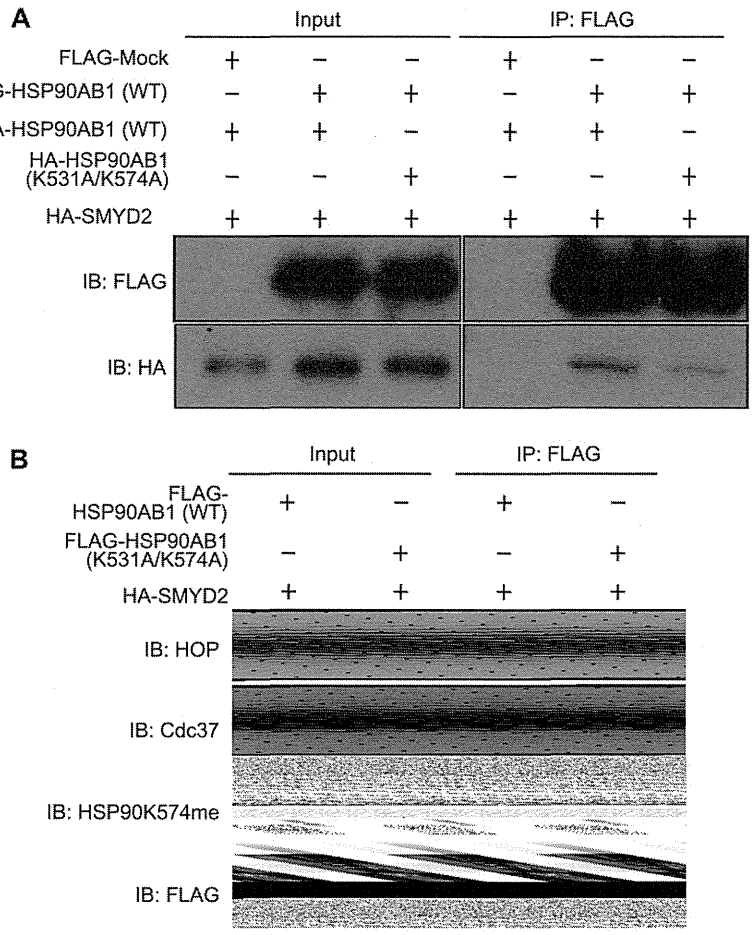


**Fig. 5.** Methylation is vital for formation of the HSP90AB1 chaperon complex. (A) 293T cells were co-transfected with FLAG-Mock or FLAG-HSP90AB1 (WT) and HA-HSP90AB1 (WT or K531A/K574A) expression vectors in the presence of a HA-SMYD2 expression vector. Immunoprecipitation was performed using anti-FLAG® M2 agarose beads, and samples were immunoblotted with anti-FLAG and anti-HA antibodies. The result was replicated three times. (B) 293T cells were transfected with a FLAG-HSP90AB1 (WT) expression vector or a FLAG-HSP90AB1 (K531A/K574A) expression vector in the presence of an HA-SMYD2 expression vector. Immunoprecipitation was performed anti-FLAG® M2 agarose beads, and samples were immunoblotted with anti-HOP, anti-Cdc37, anti-p23, anti-HSP90meK574me1 and anti-FLAG antibodies. The result was replicated three times.

facilitate the formation of chaperone complex of HSP90AB1 and promote cancer cell growth, and thereby contributes to human carcinogenesis.

## Discussion

We previously reported that several histone methyltransferases (HMTs) play a vital role in human cancer pathogenesis [17,30–33]. Other groups have also indicated involvement of HMTs in human carcinogenesis [34–36]. These pieces of evidence clearly indicate that deregulation of HMTs is very common features in human cancers, but the biological mechanisms of HMT abnormalities in human cancer cells still remains to be clarified. We recently reported that SMYD2 was overexpressed in various cancer tissues including bladder cancer [14]. In this study, we have demonstrated that SMYD2 methylates HSP90AB1 and effects on the HSP90 functions, further implying the critical role of methylation of non-histone proteins by histone methyltransferases. Multiple studies reveal that methylation of non-histone proteins results in various effects including subcellular localization, protein stability and binding affinity to interacting partners [17,37–39]. In the present study, we clarified that methylation of HSP90AB1 by SMYD2 caused various effects including the chaperone complex formation and then promoted cancer cell proliferation (Figs. 5 and 6).

HSP90 is ubiquitously expressed in eukaryotic cells and consists of three domains, the N-domain (ATP binding pocket), the M-domain (binding regions for co-chaperones and client proteins) and the C-terminal dimerization motif [2]. HSP90 serves as an evolutionarily conserved molecular chaperone that assists a number of newly synthesized polypeptides and unstable folded proteins to fold correctly and prevent them misaggregating [2,25]. Since HSP90-client proteins include transcriptional factors and proteins kinases which are crucial for signal transduction and adaptive responses to various stresses, HSP90 appears to have an essential role in regulating multiple cellular functions [40,41]. To exert chaperone functions, homo-dimerization and coordination with co-chaperone proteins such as p21, HOP and Cdc37 are essential [26,42]. Client proteins are clamped by ATP-bound HSP90 protein, and the folding process is conducted by HSP90 in cooperation with other chaperones and co-chaperones, followed by release of the matured clients which depend on conformational changes to HSP90 fueled by ATP hydrolysis [43–45]. There are some reports for HSP90 functions regulated by multiple PTMs such as phosphorylation and acetylation [7,11,23,24], but the methylation of HSP90 has still been investigated [46,47]. Abu-Farha et al. recently reported that SMYD2 could methylate K209 and K615 on HSP90 alpha (HSPAA1) nucleotide-binding and dimerization domain, respectively [46]. In addition, Donlin et al. demonstrated the importance of HSP90 methylation by SMYD2 for muscle functions

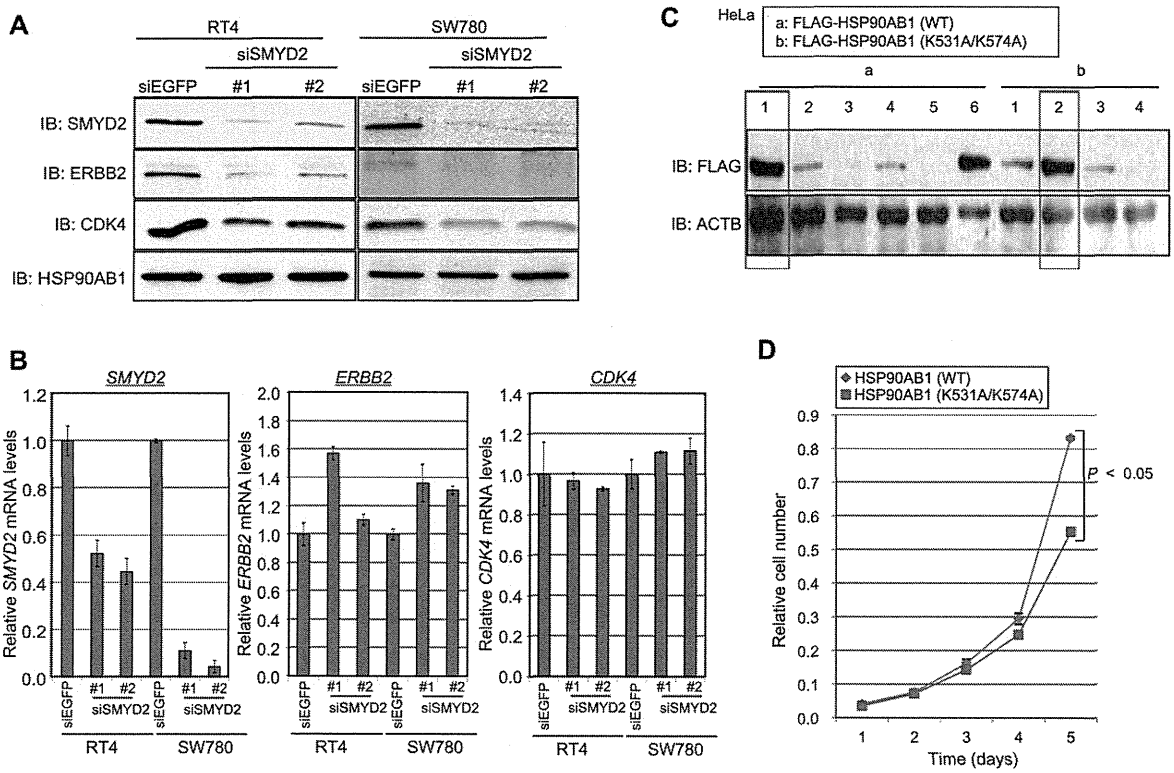


**Fig. 6.** SMYD2-dependent HSP90AB1 methylation promotes the growth of cancer cells. (A) RT4 and SW780 cells were treated with siEGFP, siSMYD2#1 and siSMYD2#2, and cells were harvested 72 h after the transfection. Western blot was conducted using anti-SMYD2 (#9734, Cell Signaling Technology), anti-ERBB2 (#2248, Cell Signaling Technology), anti-CDK4 (#12790, Cell Signaling Technology) and anti-HSP90AB1 (#5087, Cell Signaling Technology) antibodies. The result was replicated three times. (B) Relative *SMYD2*, *ERBB2* and *CDK4* mRNA expression levels analyzed by real-time PCR. RNA was purified 72 h after treatment with siEGFP, siSMYD2#1 and siSMYD2#2. *GAPDH* was used as a housekeeping gene. Results are the mean ± SD of three independent experiments. (C) Validation of HSP90AB1 (WT or K531A/K574A) expression in HeLa cells stably expressing FLAG-HSP90AB1 (WT or K531A/K574A). HeLa cells stably expressing FLAG-HSP90 (WT or K531A/K574A) were constructed and lysates were immunoblotted with anti-FLAG and anti-ACTB (an internal control) antibodies. (D) The cell growth assay was performed every 24 h using Cell Counting kit 8. Relative cell number shows the number of the cells calculated by fluorescence microplate reader (ARVO X3, Perkin Elmer): results are the mean ± SD of three independent experiments. *P* values were calculated using Student's *t*-test (**P* < 0.05).

using zebrafish [47]. In the present study, we found the novel methylation sites of HSP90AB1 and their significance in human cancer cells. Further functional analysis may unveil the physiological importance of HSP90 methylation in more detail.

A large amount of HSP90 complexes are present in cancer cells than in normal cells [48] and this cancer-specific chaperone machinery is likely to protect oncoproteins in cancer cells from misfolding and proteasomal degradation [1]. This suggests that increased HSP90 chaperone complexes are intimately involved in human oncogenesis, and our results imply that the tumor-specific abnormality of the HSP90 chaperone complex formation appears to be caused partly by SMYD2-dependent methylation in cancer cells. Hence, HSP90 methylation by SMYD2 is likely to be one of the fundamental processes of human carcinogenesis.

Although dozens of novel possible druggable targets have been identified and newly-emerging drugs are undergoing clinical trials, current molecular targeting drugs do not ensure satisfying outcomes in most of the cases, and adverse events are not negligible [49,50]. Therefore, it is crucial to discover ideal therapeutic targets to extend the capability of cancer treatment. In this regard, we previously found expression levels of SMYD2 in various types of cancer tissues to be significantly higher than those in corresponding non-neoplastic tissues, and knockdown of SMYD2 significantly suppressed the growth of cancer cells [14]. Taken together with another report [16], SMYD2 is likely to play an important role in human carcinogenesis. Considering recent development of novel HMTs inhibitors, SMYD2 should also be one of the ideal therapeutic targets in cancer for development of drugs with lower risk to cause adverse events due to its very low expression in normal cells.

## Conflict of Interest

R. Hamamoto, M. Nakakido and Y. Nakamura have Research Grants from Oncotherapy Science, Inc. No potential conflicts of interest are disclosed by the other authors.

## Acknowledgements

We thank Drs. Masanori Yoshimatsu, Hyun-Soo Cho, Vassiliki Saloura, Kenbun Sone and Lianhua Piao for helpful discussion and their technical supports. This work was supported by a Grant-in Aid for Young Scientists (A) (22681030) from the Japan Society for the Promotion of Science and Project for Development of Innovation Research on Cancer Therapeutics.

## Appendix A. Supplementary material

Supplementary data associated with this article can be found, in the online version, at http://dx.doi.org/10.1016/j.canlet.2014.05.014.

## References

[1] J. Trepel, M. Mollapour, G. Giaccone, L. Neckers, Targeting the dynamic HSP90 complex in cancer, Nat. Rev. Cancer 10 (2010) 537–549.
[2] S.K. Wandinger, K. Richter, J. Buchner, The Hsp90 chaperone machinery, J. Biol. Chem. 283 (2008) 18473–18477.
[3] W.B. Pratt, D.O. Toft, Regulation of signaling protein function and trafficking by the hsp90/hsp70-based chaperone machinery, Exp. Biol. Med. (Maywood) 228 (2003) 111–133.

[4] L. Whitesell, S.L. Lindquist, HSP90 and the chaperoning of cancer, Nat. Rev. Cancer 5 (2005) 761–772.
[5] H. Ogiso, N. Kagi, E. Matsumoto, M. Nishimoto, R. Arai, M. Shirouzu, J. Mimura, Y. Fujii-Kuriyama, S. Yokoyama, Phosphorylation analysis of 90 kDa heat shock protein within the cytosolic arylhydrocarbon receptor complex, Biochemistry 43 (2004) 15510–15519.
[6] M. Duval, F. Le Boeuf, J. Huot, J.P. Gratton, Src-mediated phosphorylation of Hsp90 in response to vascular endothelial growth factor (VEGF) is required for VEGF receptor-2 signaling to endothelial NO synthase, Mol. Biol. Cell 18 (2007) 4659–4668.
[7] B.T. Scroggins, K. Robzyk, D. Wang, M.G. Marcu, S. Tsutsumi, K. Beebe, R.J. Cotter, S. Felts, D. Toft, L. Karnitz, N. Rosen, L. Neckers, An acetylation site in the middle domain of Hsp90 regulates chaperone function, Mol. Cell 25 (2007) 151–159.
[8] J.J. Kovacs, P.J. Murphy, S. Gaillard, X. Zhao, J.T. Wu, C.V. Nicchitta, M. Yoshida, D.O. Toft, W.B. Pratt, T.P. Yao, HDAC6 regulates Hsp90 acetylation and chaperone-dependent activation of glucocorticoid receptor, Mol. Cell 18 (2005) 601–607.
[9] J. Ai, Y. Wang, J.A. Dar, J. Liu, L. Liu, J.B. Nelson, Z. Wang, HDAC6 regulates androgen receptor hypersensitivity and nuclear localization via modulating Hsp90 acetylation in castration-resistant prostate cancer, Mol. Endocrinol. 23 (2009) 1963–1972.
[10] M. Retzlaff, M. Stahl, H.C. Eberl, S. Lagleder, J. Beck, H. Kessler, J. Buchner, Hsp90 is regulated by a switch point in the C-terminal domain, EMBO Rep. 10 (2009) 1147–1153.
[11] A. Martinez-Ruiz, L. Villanueva, C. Gonzalez de Orduna, D. Lopez-Ferrer, M.A. Higueras, C. Tarin, I. Rodriguez-Crespo, J. Vazquez, S. Lamas, S-nitrosylation of Hsp90 promotes the inhibition of its ATPase and endothelial nitric oxide synthase regulatory activities, Proc. Natl. Acad. Sci. U. S. A. 102 (2005) 8525–8530.
[12] M.A. Brown, R.J. Sims 3rd, P.D. Gottlieb, P.W. Tucker, Identification and characterization of Smyd2: a split SET/MYND domain-containing histone H3 lysine 36-specific methyltransferase that interacts with the Sin3 histone deacetylase complex, Mol. Cancer 5 (2006) 26.
[13] M. Abu-Farha, J.P. Lambert, A.S. Al-Madhoun, F. Elisma, I.S. Skerjanc, D. Figeys, The tale of two domains: proteomics and genomics analysis of SMYD2, a new histone methyltransferase, Mol. Cell. Proteomics: MCP 7 (2008) 560–572.
[14] H.S. Cho, S. Hayami, G. Toyokawa, K. Maejima, Y. Yamane, T. Suzuki, N. Dohmae, M. Kogure, D. Kang, D.E. Neal, B.A. Ponder, H. Yamaue, Y. Nakamura, R. Hamamoto, RB1 methylation by SMYD2 enhances cell cycle progression through an increase of RB1 phosphorylation, Neoplasia 14 (2012) 476–486.
[15] J. Huang, L. Perez-Burgos, B.J. Placek, R. Sengupta, M. Richter, J.A. Dorsey, S. Kubicek, S. Opravil, T. Jenuwein, S.L. Berger, Repression of p53 activity by Smyd2-mediated methylation, Nature 444 (2006) 629–632.
[16] S. Komatsu, I. Imoto, H. Tsuda, K.I. Kozaki, T. Muramatsu, Y. Shimada, S. Aiko, Y. Yoshizumi, D. Ichikawa, E. Otsuji, J. Inazawa, Overexpression of SMYD2 relates to tumor cell proliferation and malignant outcome of esophageal squamous cell carcinoma, Carcinogenesis 30 (2009) 1139–1146.
[17] H.S. Cho, T. Shimazu, G. Toyokawa, Y. Daigo, Y. Maehara, S. Hayami, A. Ito, K. Masuda, N. Ikawa, H.I. Field, E. Tsuchiya, S. Ohnuma, B.A. Ponder, M. Yoshida, Y. Nakamura, R. Hamamoto, Enhanced HSP70 lysine methylation promotes proliferation of cancer cells through activation of aurora kinase B, Nat. Commun. 3 (2012) 1072.
[18] M. Takawa, H.S. Cho, S. Hayami, G. Toyokawa, M. Kogure, Y. Yamane, Y. Iwai, K. Maejima, K. Ueda, A. Masuda, N. Dohmae, H.I. Field, T. Tsunoda, T. Kobayashi, T. Akasu, M. Sugiyama, S.I. Ohnuma, Y. Atomi, B.A. Ponder, Y. Nakamura, R. Hamamoto, Histone lysine methyltransferase SETD8 promotes carcinogenesis by deregulating PCNA expression, Cancer Res. 72 (2012) 3217–3227.
[19] H.S. Cho, T. Suzuki, N. Dohmae, S. Hayami, M. Unoki, M. Yoshimatsu, G. Toyokawa, M. Takawa, T. Chen, J.K. Kurash, H. Field, B.A. Ponder, Y. Nakamura, R. Hamamoto, Demethylation of RB regulator MYPT1 by histone demethylase LSD1 promotes cell cycle progression in cancer cells, Cancer Res. (2010).
[20] S. Hayami, J.D. Kelly, H.S. Cho, M. Yoshimatsu, M. Unoki, T. Tsunoda, H.I. Field, D.E. Neal, H. Yamaue, B.A. Ponder, Y. Nakamura, R. Hamamoto, Overexpression of LSD1 contributes to human carcinogenesis through chromatin regulation in various cancers, Int. J. Cancer 128 (2011) 574–586.
[21] S. Hayami, M. Yoshimatsu, A. Veerakumarasivam, M. Unoki, Y. Iwai, T. Tsunoda, H.I. Field, J.D. Kelly, D.E. Neal, H. Yamaue, B.A. Ponder, Y. Nakamura, R. Hamamoto, Overexpression of the JmjC histone demethylase KDM5B in human carcinogenesis: involvement in the proliferation of cancer cells through the E2F/RB pathway, Mol. Cancer 9 (2010) 59.
[22] R.K. Allan, D. Mok, B.K. Ward, T. Ratajczak, Modulation of chaperone function and cochaperone interaction by novobiocin in the C-terminal domain of Hsp90: evidence that coumarin antibiotics disrupt Hsp90 dimerization, J. Biol. Chem. 281 (2006) 7161–7171.
[23] M. Mollapour, S. Tsutsumi, A.C. Donnelly, K. Beebe, M.J. Tokita, M.J. Lee, S. Lee, G. Morra, D. Bourboulia, B.T. Scroggins, G. Colombo, B.S. Blagg, B. Panaretou, W.G. Stetler-Stevenson, J.B. Trepel, P.W. Piper, C. Prodromou, L.H. Pearl, L. Neckers, Swe1Wee1-dependent tyrosine phosphorylation of Hsp90 regulates distinct facets of chaperone function, Mol. Cell 37 (2010) 333–343.
[24] M. Mollapour, S. Tsutsumi, A.W. Truman, W. Xu, C.K. Vaughan, K. Beebe, A. Konstantinova, S. Vourganti, B. Panaretou, P.W. Piper, J.B. Trepel, C. Prodromou, L.H. Pearl, L. Neckers, Threonine 22 phosphorylation attenuates Hsp90 interaction with cochaperones and affects its chaperone activity, Mol. Cell 41 (2011) 672–681.
[25] J.C. Young, V.R. Agashe, K. Siegers, F.U. Hartl, Pathways of chaperone-mediated protein folding in the cytosol, Nat. Rev. Mol. Cell Biol. 5 (2004) 781–791.
[26] M. Taipale, D.F. Jarosz, S. Lindquist, HSP90 at the hub of protein homeostasis: emerging mechanistic insights, Nat. Rev. Mol. Cell Biol. 11 (2010) 515–528.
[27] M.P. Mayer, Phosphotyrosine confers client specificity to Hsp90, Mol. Cell 37 (2010) 295–296.
[28] R.Q. Miao, J. Fontana, D. Fulton, M.I. Lin, K.D. Harrison, W.C. Sessa, Dominant-negative Hsp90 reduces VEGF-stimulated nitric oxide release and migration in endothelial cells, Arterioscler. Thromb. Vasc. Biol. 28 (2008) 105–111.
[29] A. Zurawska, J. Urbanski, J. Matuliene, J. Baraniak, M.P. Klejman, S. Filipek, D. Matulis, P. Bieganowski, Mutations that increase both Hsp90 ATPase activity in vitro and Hsp90 drug resistance in vivo, Biochim. Biophys. Acta 2010 (1803) 575–583.
[30] R. Hamamoto, Y. Furukawa, M. Morita, Y. Iimura, F.P. Silva, M. Li, R. Yagyu, Y. Nakamura, SMYD3 encodes a histone methyltransferase involved in the proliferation of cancer cells, Nat. Cell Biol. 6 (2004) 731–740.
[31] M. Takawa, K. Masuda, M. Kunizaki, Y. Daigo, K. Takagi, Y. Iwai, H.S. Cho, G. Toyokawa, Y. Yamane, K. Maejima, H.I. Field, T. Kobayashi, T. Akasu, M. Sugiyama, E. Tsuchiya, Y. Atomi, B.A. Ponder, Y. Nakamura, R. Hamamoto, Validation of the histone methyltransferase EZH2 as a therapeutic target for various types of human cancer and as a prognostic marker, Cancer Sci. (2011).
[32] M. Yoshimatsu, G. Toyokawa, S. Hayami, M. Unoki, T. Tsunoda, H.I. Field, J.D. Kelly, D.E. Neal, Y. Maehara, B.A. Ponder, Y. Nakamura, R. Hamamoto, Dysregulation of PRMT1 and PRMT6, Type I arginine methyltransferases, is involved in various types of human cancers, Int. J. Cancer 128 (2011) 562–573.
[33] R. Hamamoto, F.P. Silva, M. Tsuge, T. Nishidate, T. Katagiri, Y. Nakamura, Y. Furukawa, Enhanced SMYD3 expression is essential for the growth of breast cancer cells, Cancer Sci. 97 (2006) 113–118.
[34] A. Portela, M. Esteller, Epigenetic modifications and human disease, Nat. Biotechnol. 28 (2010) 1057–1068.
[35] R. Schneider, A.J. Bannister, T. Kouzarides, Unsafe SETs: histone lysine methyltransferases and cancer, Trends Biochem. Sci. 27 (2002) 396–402.
[36] A. Sparmann, M. van Lohuizen, Polycomb silencers control cell fate, development and cancer, Nat. Rev. Cancer 6 (2006) 846–856.
[37] P.O. Esteve, H.G. Chin, J. Benner, G.R. Feehery, M. Samaranayake, G.A. Horwitz, S.E. Jacobsen, S. Pradhan, Regulation of DNMT1 stability through SET7-mediated lysine methylation in mammalian cells, Proc. Natl. Acad. Sci. U. S. A. 106 (2009) 5076–5081.
[38] Z. Guo, L. Zheng, H. Xu, H. Dai, M. Zhou, M.R. Pascua, Q.M. Chen, B. Shen, Methylation of FEN1 suppresses nearby phosphorylation and facilitates PCNA binding, Nat. Chem. Biol. 6 (2010) 766–773.
[39] H.S. Cho, T. Suzuki, N. Dohmae, S. Hayami, M. Unoki, M. Yoshimatsu, G. Toyokawa, M. Takawa, T. Chen, J.K. Kurash, H.I. Field, B.A. Ponder, Y. Nakamura, R. Hamamoto, Demethylation of RB regulator MYPT1 by histone demethylase LSD1 promotes cell cycle progression in cancer cells, Cancer Res. 71 (2011) 1–6.
[40] R. Zhao, M. Davey, Y.C. Hsu, P. Kaplanek, A. Tong, A.B. Parsons, N. Krogan, G. Cagney, D. Mai, J. Greenblatt, C. Boone, A. Emili, W.A. Houry, Navigating the chaperone network: an integrative map of physical and genetic interactions mediated by the hsp90 chaperone, Cell 120 (2005) 715–727.
[41] G. Chiosis, M. Vilenchik, J. Kim, D. Solit, Hsp90: the vulnerable chaperone, Drug Discov. Today 9 (2004) 881–888.
[42] N. Wayne, D.N. Bolon, Dimerization of Hsp90 is required for in vivo function, Des. Anal. Monomers Dimers J. Biol. Chem. 282 (2007) 35386–35395.
[43] M.M. Ali, S.M. Roe, C.K. Vaughan, P. Meyer, B. Panaretou, P.W. Piper, C. Prodromou, L.H. Pearl, Crystal structure of an Hsp90-nucleotide-p23/Sba1 closed chaperone complex, Nature 440 (2006) 1013–1017.
[44] C.K. Vaughan, U. Gohlke, F. Sobott, V.M. Good, M.M. Ali, C. Prodromou, C.V. Robinson, H.R. Saibil, L.H. Pearl, Structure of an Hsp90-Cdc37-Cdk4 complex, Mol. Cell 23 (2006) 697–707.
[45] M. Hessling, K. Richter, J. Buchner, Dissection of the ATP-induced conformational cycle of the molecular chaperone Hsp90, Nat. Struct. Mol. Biol. 16 (2009) 287–293.
[46] M. Abu-Farha, S. Lanouette, F. Elisma, V. Tremblay, J. Butson, D. Figeys, J.F. Couture, Proteomic analyses of the SMYD family interactomes identify HSP90 as a novel target for SMYD2, J. Mol. Cell Biol. 3 (2011) 301–308.
[47] L.T. Donlin, C. Andresen, S. Just, E. Rudensky, C.T. Pappas, M. Kruger, E.Y. Jacobs, A. Unger, A. Zieseniss, M.W. Dobenecker, T. Voelkel, B.T. Chait, C.C. Gregorio, W. Rottbauer, A. Tarakhovsky, W.A. Linke, Smyd2 controls cytoplasmic lysine methylation of Hsp90 and myofilament organization, Genes Dev. 26 (2012) 114–119.
[48] A. Kamal, L. Thao, J. Sensintaffar, L. Zhang, M.F. Boehm, L.C. Fritz, F.J. Burrows, A high-affinity conformation of Hsp90 confers tumour selectivity on Hsp90 inhibitors, Nature 425 (2003) 407–410.
[49] P.C. Black, P.K. Agarwal, C.P. Dinney, Targeted therapies in bladder cancer–an update, Urol. Oncol. 25 (2007) 433–438.
[50] G. Sonpavde, C.N. Sternberg, J.E. Rosenberg, N.M. Hahn, M.D. Galsky, N.J. Vogelzang, Second-line systemic therapy and emerging drugs for metastatic transitional-cell carcinoma of the urothelium, Lancet Oncol. 11 (2010) 861–870.

# Identification of a nuclear protein, LRRC42, involved in lung carcinogenesis

TAKASHI FUJITOMO[1], YATARO DAIGO[1,2], KOICHI MATSUDA[1], KOJI UEDA[3] and YUSUKE NAKAMURA[1,4]

[1]Laboratory of Molecular Medicine, Human Genome Center, Institute of Medical Science, The University of Tokyo, Tokyo 108-8639; [2]Department of Medical Oncology and Cancer Center, Shiga University of Medical Science, Otsu 520-2192; [3]Laboratory for Biomarker Development, Center for Genomic Medicine, RIKEN, Yokohama 230-0045, Japan; [4]Department of Medicine, The University of Chicago, 5801 South Ellis Avenue, Chicago, IL 60637, USA

DOI: 10.3892/ijo_xxxxxxxx

**Abstract.** On the basis of the gene expression profiles of 120 lung cancer cases using a cDNA microarray containing 27,648 genes or expressed sequence tags (ESTs), we identified *LRRC42* (Leucine-rich repeat containing 42) to be significantly upregulated in the majority of lung cancers. Northern blot analysis demonstrated that *LRRC42* was expressed only in testis among normal tissues examined. Knockdown of LRRC42 expression by siRNA against LRRC42 significantly suppressed the growth of lung cancer cells. On the other hand, stable induction of LRRC42 expression significantly promoted cell growth. LRRC42, which was found to localize in the nucleus of mammalian cells, is likely to interact with and stabilize GATAD2B (GATA zinc finger domain-containing 2B) and MBD3 (Methyl-CpG-binding domain protein 3) proteins that could contribute to lung cancer cell proliferation partly through the regulation of $p21^{Waf1/Cip1}$. Our findings suggest that LRRC42 overexpression as well as its interaction with LRRC42-GATAD2B might play essential roles in lung carcinogenesis, and be a promising molecular target for lung cancer therapy.

## Introduction

Lung cancer is the leading cause of cancer-related death worldwide. Despite some advances in cancer diagnostics and recent improvements in its treatment, the overall 5-year survival rate is still only 15% (1). Several oncogenic alterations, such as *KRAS* and *EGFR* mutations, and *EML4-ALK* fusion genes as well as inactivation of tumor suppressor gene of *TP53* in lung cancer have been reported, however the precise molecular mechanisms of pulmonary carcinogenesis are still far from fully understood (2). Although several molecular targeted-drugs such as gefitinib, bevacizumab and crizotinib have been approved for lung cancer treatment, the portion of patients who are able to have the benefit of these drugs is still limited and several serious adverse reactions such as interstitial pneumonia by gefitinib and hemorrhage by bevacizumab have been reported (3,4). Hence, the development of molecular targeted agents providing better clinical benefits with less adverse events are eagerly required.

Systematic analysis of expression levels of thousands of genes using a cDNA microarray is an effective technique to identify molecules involved in carcinogenic pathways (5); some of such genes or their gene products may be good molecular targets for the development of novel therapies and/or cancer biomarkers. To isolate potential molecular targets for diagnosis, treatment, and/or prevention of lung carcinomas, we performed a genome-wide analysis of gene expression profiles of tumor tissues from 120 lung cancer cases by means of cDNA microarray consisting of 27,648 genes or expressed sequence tags (ESTs) (6-10). Among the transactivated genes, we identified *LRRC42* (Leucine-rich repeat containing 42) as a potential therapeutic target for lung cancer. LRRC42 protein contains two leucine-rich repeats (LRRs) which are widespread structural motifs comprising 20-30 amino acids with a characteristic repetitive sequence pattern rich in leucine residues. Leucine-rich repeat domains are built from tandems of two or more repeats and form curved solenoid structures that are particularly suitable for protein-protein interactions. LRR-containing proteins participate in many important biological processes, including plant and animal immunity, hormone-receptor interactions, cell adhesion, signal transduction, regulation of gene expression and apoptosis (11-14). However, the pathophysiological roles of LRRC42 in cancer cells have not been reported. Herein we report identification of LRRC42 as a potential therapeutic target and also provide evidence that LRRC42 could interact with GATAD2B (GATA zinc finger domain containing 2B) and MBD3 (Methyl-CpG-binding domain protein 3) proteins that are likely to play a significant role in human pulmonary carcinogenesis.

*Correspondence to:* Professor Yusuke Nakamura, Department of Medicine and Surgery, The University of Chicago, Knapp Center for Biomedical Discovery, 900 E. 57th Street, KCBD6130, Chicago, IL 60637, USA
E-mail: ynakamura@bsd.uchicago.edu

*Key words:* oncogene, cancer-testis antigen, therapeutic target, lung cancer, novel molecular target

## Materials and methods

*Lung cancer cell lines and tissue samples.* The human lung cancer cell lines used in this study were as follows: A549, NCI-H1373, NCI-H1781, SKMES-1, NCI-H520, NCI-H1703, NCI-H2170 and DMS114 were distributed from America Type Culture Collection (ATCC, Manassas, VA, USA). LC319 was kindly provided from Aichi Cancer Center (Aichi, Japan). PC14 was obtained from RIKEN BioRsource Center (Ibaraki, Japan). LU61 and LX1 were obtained from Central Institute for Experimental Animals (Kanagawa, Japan). DMS273 was obtained from European Collection of Animal Cell Cultures (ECACC, Salisbury, UK). SBC-3 and SBC-5 were obtained from Japanese Collection of Research Bioresources (JCRB, Osaka, Japan). All cells were grown in monolayers in appropriate medium supplemented with 10% FCS and were maintained at 37°C in atmospheres of humidified air with 5% $CO_2$. Human small airway epithelial cells (SAEC) were grown in optimized medium purchased from Cambrex Bio Science, Inc. (Walkersville, MD, USA). Primary lung cancer tissue samples were obtained with informed consent as previously described (6,10). This study was approved by individual institutional ethical committees.

*Quantitative real-time PCR.* Total RNA was extracted from cultured cells using the QIAshredder (Qiagen, Valencia, CA, USA) and RNeasy® Plus mini kit (Qiagen) according to the manufacturer's protocol. Extracted RNAs were reverse transcribed using oligo (dT) primer (Life Technologies, Carlsbad, CA, USA) and SuperScript III (Life Technologies). Quantitative real-time PCR was conducted with the SYBR Green I Master kit on a LightCycler 480 (Roche Diagnostics, Mannheim, Germany) according to the manufacturer's recommendations. Each experiment was done in duplicate. *GAPDH* was used for normalization of expression levels. For quantitative RT-PCR reactions, specific primers for all human *LRRC42, GATAD2B, MBD3, p21$^{Waf1/Cip1}$* and *GAPDH* were designed as follows: *LRRC42*, 5'-TTGATCATAGTAACTGCAAGACAGAG-3' and 5'-ACGCTCCCACTGCAGAAC-3'; *GARAD2B*, 5'-CACCAACCGGCTGAAAAAT-3' and 5'-GCTGCT GTAATCGCTGTTCA-3', *MBD3*, 5'-ACCATGGACC TCCCCAAG-3' and 5'-CGACAGCAGCGTCTCATC-3'; *p21$^{Waf1/Cip1}$*, 5'-GACCTGTCACTGTCTTGTACCC-3' and 5'-AAGATCAGCCGGCGTTTG-3'; *GAPDH*, 5'-ACCATG GGGAAGGTGAAG-3' and 5'-AATGAAGGGGTCATT GATGG-3'.

*Immunofluorescence analysis.* Cells were plated onto glass coverslips (Becton Dickinson, Mountain View, CA, USA), fixed with 4% paraformaldehyde, and permeablilized with 0.1% Triton X-100 in PBS for 5 min at room temperature. Non-specific binding was blocked by 5% skim milk for 10 min at room temperature. Cells were then incubated overnight at 4°C with primary antibodies for mouse monoclonal anti-Flag antibody (Catalog no. F3165, Sigma, St. Louis, MO, USA) and anti-GATAD2B antibody (Catalog no. HPA017015, ATLAS, Stockholm, Sweden) diluted in PBS containing 1% BSA. After being washed with PBS, the cells were stained with Alexa Fluor 488-conjugated secondary antibody (Molecular Probes, Eugene, OR, USA) (Fig. 1C), or with Alexa Fluor 488-conjugated secondary antibody and Alexa Fluor 594-conjugated secondary antibody (Molecular Probes) (Fig. 3C) for 60 min at room temperature. After another wash with PBS, each specimen was mounted with Vectashield (Vector Laboratories, Burlingame, CA, USA) containing 4', 6'-diamidine-2'-phenylindolendihydrochrolide (DAPI) and visualized with Spectral Confocal Scanning Systems (TSC SP2 AOBS: Leica Microsystems, Wetzlar, Germany).

*Northern blot analysis.* Human multiple-tissue blots (Clontech, Carlsbad, CA, USA) were hybridized with $^{32}$P-labeled PCR products of *LRRC42*. The cDNA probe of *LRRC42* was prepared by RT-PCR using following primers: *LRRC42*, 5'-GACCAGATCGTTCTGCAGTG-3' and 5'-CCTCCCA CACCACAAAAGTA-3'. Prehybridization, hybridization, and washing were performed according to the supplier's recommendations. The blots were autoradiographed at -80°C for 14 days.

*RNA interference assay.* To evaluate the biological functions of LRRC42 in lung cancer cells, we used small interfering RNA (siRNA) duplexes against the target genes (Sigma). The target sequences of the synthetic oligonucleotides for RNA interference were as follows: control-1: [EGFP, enhanced green fluorescence protein (GFP) gene, a mutant of *Aequorea gictoria* GFP], 5'-GAAGCAGCACGACUUCUUC-3'; control-2 (LUC, luciferase gene from *Photinus pyralis*), 5'-CGUACG CGGAAUACUUCGA-3'; si-LRRC42-#1, 5'-CUUACUA CCUCAGCUCAGA-3'; si-LRRC42-#2, 5'-GACUUGUUA AAUUCCUAUU-3'; si-GATAD2B, 5'-GCCAAUAGCG AGUUCAUCU-3'; si-MBD3, 5'-CACAGUCGAGGCACG UCAU-3'. Lung cancer cell lines, LC319 and SBC-3, were plated onto 10-cm dishes ($5.0x10^5$ per dish), and transfected with either of the siRNA oligonucleotides (50 $\mu$M) using 30 $\mu$l of Lipofectamine® RNAiMAX (Life Technologies) according to the manufacturers' instructions. After seven days of incubation, the cells were stained by Giemsa solution to assess colony formation, and cell numbers were assessed by Cell Counting Kit-8 (Dojindo Co., Kumamoto, Japan); briefly, Cell Counting Kit-8 solution was added to each dish at concentration of 1/10 volume, and the plates were incubated at 37°C for additional 1 h. Absorbance was then measured at 490 nm, and at 630 nm as a reference, with a 2030 ARVO™ X3 (PerkinElmer, Courtaboeuf, France).

*Anti-LRRC42 antibody.* Plasmids expressing partial LRRC42 that contained His-tagged epitopes at their $NH_2$ termini were prepared using pET28 vector (Novagen, Darmstadt, Germany) and primers LRRC42-F (5'-GGAATTCTGGGCTGA CCAGATCGTTCTGC-3') and LRRC42-R (5'-ATAGTTT AGCGGCCGCTTAGTTATTCTGTTCTGTCTCTGACT-3'. Recombinant proteins were expressed in *Escherichia coli* BL21 codon-plus strain (Stratagene, San Diego, CA, USA) and purified using Ni-NTA (Qiagen) according to the supplier's protocol. The protein was inoculated into rabbits; immune sera were purified on affinity columns according to standard methods. Affinity-purified anti-LRRC42 antibodies were used for western blotting. We confirmed that the antibody was specific to LRRC42 on western blots using lysates from cell lines that had been transfected with LRRC42 expression vector.

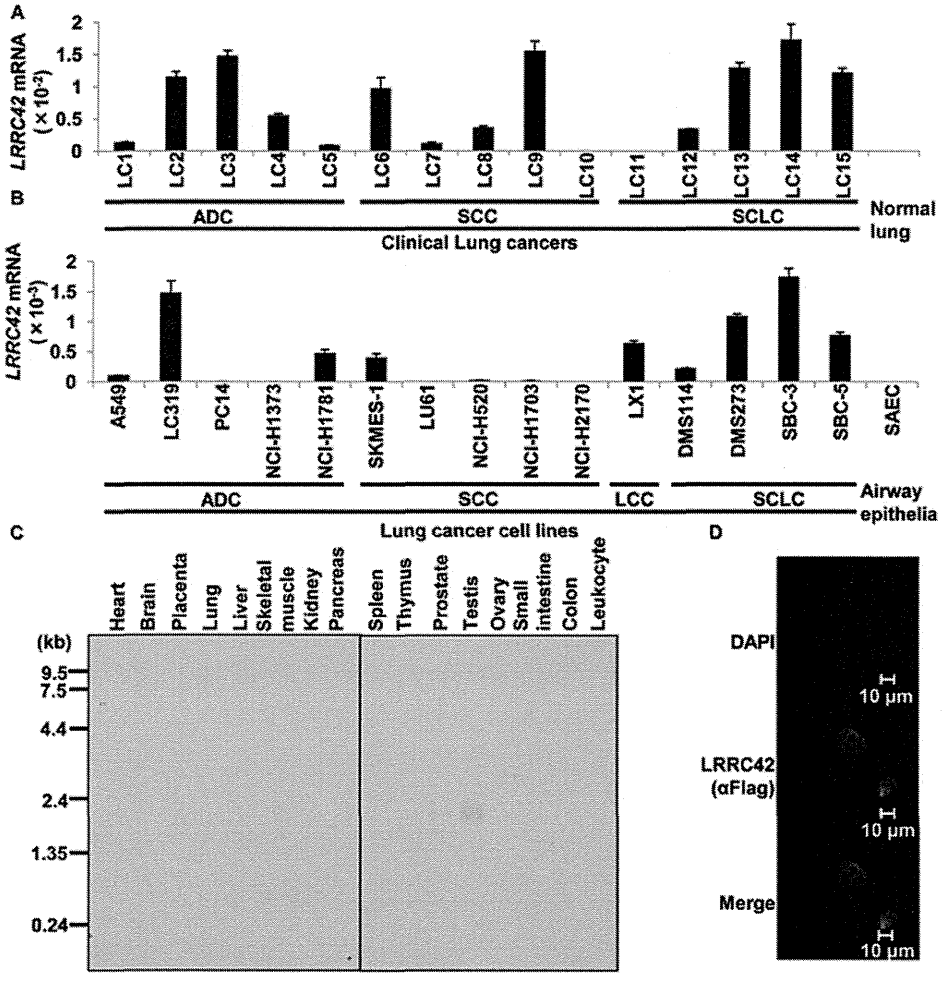


Figure 1. LRRC42 expression in lung cancers and normal tissues. (A) Expression of *LRRC42* in clinical NSCLC (non-small cell lung cancer) and SCLC (small cell clung cancer) samples, and normal lung tissues, analyzed by quantitative real-time PCR. mRNA expression levels were normalized by *GAPDH* expression. The columns and bars represent the mean and SE, respectively. (B) mRNA expression analysis of *LRRC42* in lung cancer cell lines by quantitative real-time PCR. The columns and bars represent the mean and SE, respectively. (C) Subcellular localization of exogenous LRRC42 protein in COS-7 cells detected by anti-Flag (green), which were co-stained with DAPI (blue). (D) mRNA expression analysis of *LRRC42* in normal human tissues by northern blot analysis.

*Western blotting*. Cells were lysed with immunoprecipitation assay buffer [50 mmol/l Tris-HCl (pH 8.0), 150 mmol/l NaCl, 1% NP40, 0.5% deoxychorate-Na, 0.1% SDS] containing Phosphatase Inhibitor Cocktail Set II and Protease Inhibitor Cocktail Set III EDTA-Free (Calbiochem, San Diego, CA, USA). Protein samples were separated by SDS-polyacrylamide gels and electroblotted onto Hybond-P PVDF membranes (GE Healthcare Bio-Sciences, Piscataway, NJ, USA). Blots were incubated with a mouse monoclonal anti-Flag antibody, a rabbit anti-Flag antibody (Catalog no. F7425, Sigma), an anti-GATAD2B antibody, an anti-MBD3 antibody (Catalog no. sc-9402, Santa Cruz, Santa Cruz, CA, USA), an anti-$p21^{Waf1/Cip1}$ antibody (Catalog no. 2947S, Cell Signaling, Danvers, MA, USA) and an anti-p53 antibody (Catalog no. sc-126, Santa Cruz, Santa Cruz, CA, USA). Antigen-antibody complexes were detected using secondary antibodies conjugated to horseradish peroxidase (GE Healthcare Bio-Sciences). Protein bands were visualized by enhanced chemiluminescence western blot detection reagents (GE Healthcare Bio-Sciences).

*Establishment of HEK293 cells expressing exogenous LRRC42*. T-REx HEK293 cells that could induce the expression of exogenous LRRC42 (LRRC42-HEK293) cells were generated by Flp-In expression system, where LRRC42 expression is under control of the tetracycline-regulated cytomegalovirus/$tetO_2$ hybrid promoter, and the commercially available Flp-In T-REx 293 host cell line, according to the manufacturer's instructions (Invitrogen, Carlsbad, CA, USA).

*Cell growth assay*. LRRC42-HEK293 cells were grown for four days in DMEM containing 10% FBS, Blasticidin S HCl (Life Techonologies; 15 μg/ml) and Hygromycin B (Invitrogen; 100 μg/ml) supplemented with or without doxycycline (Sigma; 100 ng/ml). Viability of cells was evaluated by Cell Counting Kit-8.

*Coimmunnoprecipitation and matrix-assisted laser desorption/ionizing-time of flight mass spectrometry mapping of LRRC42-associated proteins*. Cell extracts from lung cancer cell line SBC-3 which was transfected with LRRC42 expression (carboxyl-terminal Flag-tagged pCAGGS plasmid vector) or mock vector were precleared by incubation at 4°C for 1 h with 80 μl of protein G-agarose beads in a final volume of 200 μl of immunoprecipitation buffer (0.5% NP40, 50 mmol/l